Structure of Calcineurin bound to PI4KA reveals dual interface in both PI4KA and FAM126A

Alexandria L Shaw[1,2]*, Sushant Suresh[2]*, Matthew AH Parson[2], Noah J Harris[2], Meredith L Jenkins[2], Calvin K Yip[1], John E Burke[1,2#]

[1] Department of Biochemistry and Molecular Biology, The University of British Columbia, Vancouver, British Columbia V6T 1Z3, Canada

[2] Department of Biochemistry and Microbiology, University of Victoria, Victoria, British Columbia, V8W 2Y2, Canada

* These authors contributed equally

[#] Lead contact: John E Burke, jeburke@uvic.ca

Running title: Structure of PI4KA-Calcineurin interface

Abstract

Phosphatidylinositol 4-kinase alpha (PI4KA) maintains the PI4P and phosphatidylserine pools of the plasma membrane. A key regulator of PI4KA is its association into a complex with TTC7 and FAM126 proteins. This complex can be regulated by the CNAβ1 isoform of the phosphatase Calcineurin. We previously identified that CNAβ1 directly binds to FAM126A. Here, we report a cryo-EM structure of a truncated PI4KA complex bound to Calcineurin, revealing a direct Calcineurin interaction with PI4KA. Additional HDX-MS and computational analysis show that Calcineurin forms a complex with an evolutionarily conserved IKISVT sequence in PI4KA's horn domain. We also characterised conserved LTLT and PSISIT Calcineurin binding sequences in the C-terminus of FAM126A. These sites are in close proximity to phosphorylation sites in the PI4KA complex, suggesting key roles of Calcineurin-regulated phosphosites in PI4KA regulation. This work reveals novel insight into how Calcineurin can regulate PI4KA activity.

Keywords

PI4KA, Calcineurin, Phosphoinositides, Cryo-EM, HDX-MS, hydrogen exchange

Introduction

Phosphoinositide lipids act as master second messengers which regulate myriad cellular processes [1–3]. One of the most abundant phosphoinositides is phosphatidylinositol 4-phosphate (PI4P), with its concentration varying by cell-type, at ~1% of total cellular phospholipid [4]. PI4P is found in the cell in various subcellular membrane locations, including the Golgi, the endo-lysosomal system, and the plasma membrane (PM) [4]. PI4P is generated by the action of four different phosphatidylinositol 4-kinases [5,6], with the plasma membrane pool being primarily generated by type III phosphatidylinositol 4-kinase alpha (PI4KIIIα, which will be referred to by its gene name *PI4KA* for the remainder of the manuscript). Given the low abundance of PI at the PM [7,8], the generation of PI4P by PI4KA at the plasma membrane is essential for the generation of membrane asymmetry, partially through its critical role in controlling phosphatidylserine (PS) transport to the plasma membrane through ORP5/8 [9]. This function of PI4KA is evolutionarily conserved from yeast to humans.

PI4KA is a multi-domain protein, composed of an alpha-solenoid (horn) domain, a dimerization domain, a helical domain, and a bi-lobal kinase domain [10]. It is functional as a large multi-protein complex, primarily associated with two scaffolding proteins, TTC7 (with two possible isoforms TTC7A or TTC7B) and FAM126 (with two possible isoforms FAM126A or FAM126B) [10–12]. PI4KA and TTC7 are highly conserved throughout all eukaryotes, with FAM126 being absent in many simple unicellular eukaryotes [13,14]. The PI4KA-TTC7-FAM126 complex forms a dimer of trimers, with TTC7 and FAM126 stabilizing PI4KA, which together will be referred to as the PI4KA complex for the remainder of the manuscript [10–12]. Functionally, PI4KA is recruited to the membrane by a palmitoylated EFR3 protein (with two possible isoforms EFR3A/EFR3B [15]. The exact binding site of EFR3 to the PI4KA complex is not fully resolved but putatively involves an evolutionarily conserved C-terminal region of TTC7 [16]. PI4KA faces a complicated challenge in the generation of PI4P at the plasma membrane, as its substrate PI is present at only trace levels [7,8], with the exact mechanism of how PI4KA is regulated and activated at the plasma membrane still not fully understood.

PI4KA, TTC7, FAM126, and its accessory proteins are implicated in myriad human diseases. Intriguingly, both the loss-of-function and gain-of-function of PI4KA can be drivers of human disease [17]. Down-regulation of PI4KA signaling is observed in intestinal atresia driven by mutations in TTC7A [18], hypomyelination and congenital cataracts by a deficiency in FAM126A [19], and neurological, intestinal and immunological diseases caused by loss-of-function mutations in PI4KA [20,21].

One of the recently discovered regulators of PI4KA signaling is the protein phosphatase Calcineurin, which is a ubiquitously expressed serine/threonine phosphatase activated by Ca^{2+} signaling [22]. Calcineurin is composed of two subunits, calcineurin A (CNA) and calcineurin B (CNB), with multiple isoforms of each subunit. We have found that the lipidated CNAβ1 isoform of Calcineurin is a direct regulator of PI4KA signaling, and upon palmitoylation is recruited to the PM [23]. Cellular studies have shown that Calcineurin inhibition causes reduced PI4P synthesis following hormone-mediated $PI(4,5)P_2$ depletion, and we identified a short linear PxIxIT motif (SLiM) in FAM126A that mediates binding to CNAβ1 [23].

To fully explore the molecular mechanisms of how Calcineurin can bind to and regulate the PI4KA complex we have utilised a synergistic application of cryo-EM, hydrogen deuterium exchange mass spectrometry (HDX-MS), and AlphaFold3 modelling. Our cryo-EM structure reveals that Calcineurin not only binds the FAM126A disordered tail but also forms an evolutionarily conserved interface with the horn region of PI4KA. We used AlphaFold3 modelling to predict how PI4KA interacts with Calcineurin, with the predicted interface validated experimentally by HDX-MS. This map also had increased local resolution in the horn compared to previous cryo-EM analysis allowing for the building of a complete model of the PI4KA horn, as well as the interface between TTC7B and the N-terminus of the PI4KA horn. HDX-MS also revealed a Calcineurin binding site in a disordered loop in PI4KA's dimerization domain, which could interact with CNB's LxVP binding motif. These evolutionarily conserved PI4KA Calcineurin SLiM motifs orient the active site of Calcineurin near multiple evolutionarily conserved phosphorylation sites of unknown function. Overall, our findings provide useful insight into the molecular and structural basis of PI4KA complex regulation by Calcineurin.

89

90 ## Results and Discussion

91 ### *Cryo-EM structure of the PI4KA*-Calcineurin *complex*

92 We purified the human PI4KA complex with a truncated FAM126A tail (full-length
93 PI4KA/TTC7B and FAM126A ΔC (aa 1-308), referred to in the rest of the manuscript as
94 PI4KA complex (Fig 1A). This construct lacks the FAM126A C-terminus, which was
95 previously identified as a binding site for Calcineurin (composed of a dimer of CNA and
96 CNB subunits). We had previously observed a change in protein dynamics in the horn
97 region of PI4KA in full-length PI4KA-TTC7B-FAM126A upon binding Calcineurin [23], and
98 it was unknown if this was driven by allosteric conformational changes or acted as a direct
99 Calcineurin binding interface. To further investigate this, we purified the Calcineurin
100 heterodimer (alpha isoform of CNA with CNB) to conduct structural studies of the PI4KA-
101 Calcineurin interaction. This was done as all Calcineurin isoforms interact with their
102 substrates through the same mechanism(s) and the alpha isoform of CNA is best
103 behaved in solution and therefore more suitable for *in vitro* structural studies.

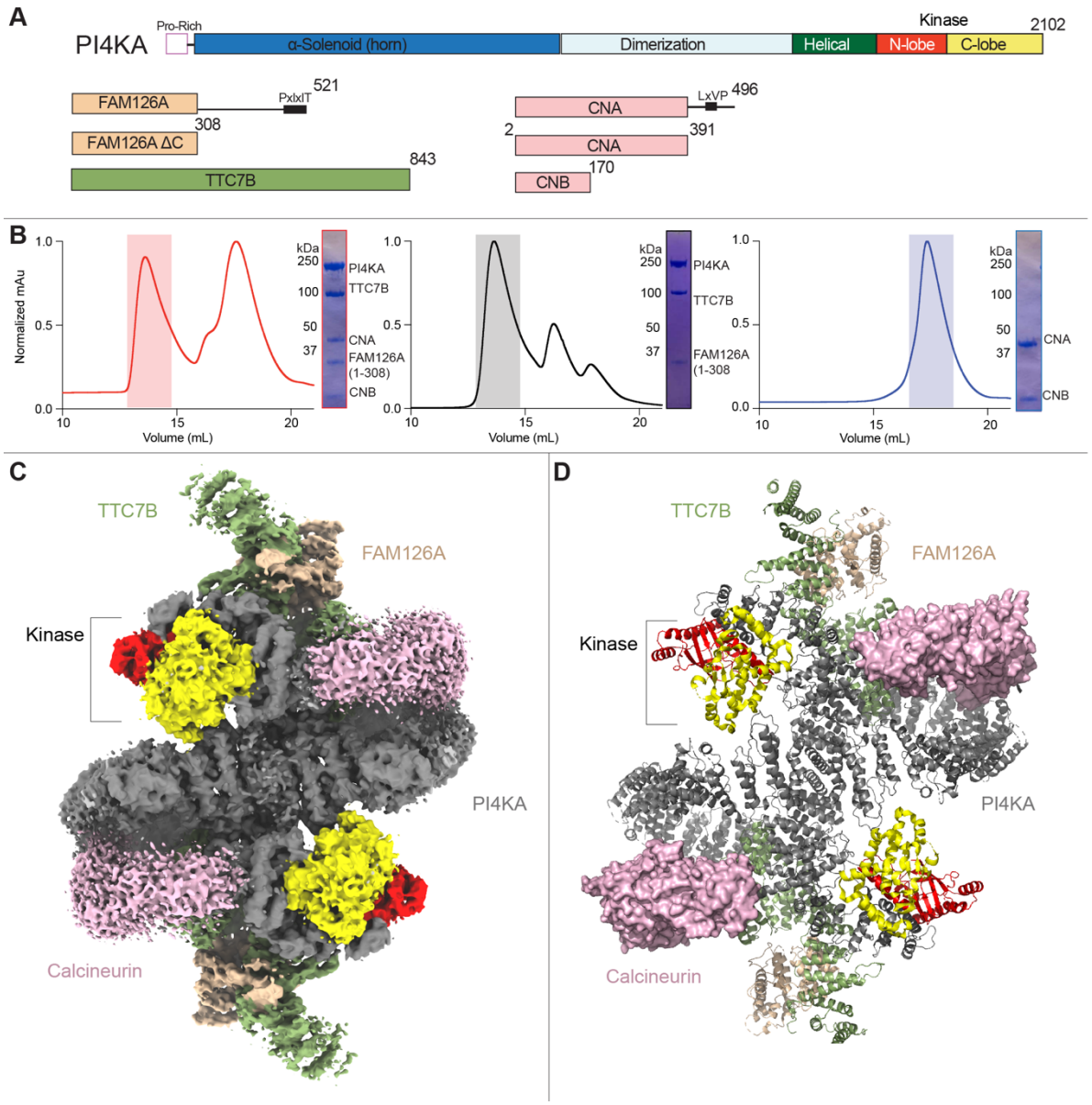

Figure 1. Calcineurin forms a complex with the PI4KA complex (see supplemental figures 1-3)

A. Domain schematics of catalytic PI4KA, regulatory proteins TTC7B and FAM126A (Full length and truncated FAM126A ΔC used in all experiments) and the serine/threonine phosphatase Calcineurin (heterodimer of CNA (top: Full length β1 isoform, bottom: truncated α1 isoform used in all experiments), and CNB).

B. Gel filtration elution profiles of PI4KA complex apo (black), Calcineurin apo (blue), or PI4KA complex bound to Calcineurin (red). SDS-polyacrylamide gel electrophoresis image of specified peaks.

C. Cryo-EM density map of the PI4KA complex bound to Calcineurin.

D. Cartoon/surface representation of the PI4KA complex bound to Calcineurin modeled from the Cryo-EM map coloured according to the in-figure text legend.

115

116 To validate if the PI4KA complex could directly interact with Calcineurin in the
117 absence of the C-terminus of FAM126A, we analysed three complexes by gel filtration:
118 PI4KA complex, Calcineurin, and the co-complex. Elution profiles were consistent with
119 the formation of a stable stochiometric dimer of pentamers (pentamer composed of
120 PI4KA, TTC7B, FAM126A ΔC, CNA, and CNB, Fig. 1B). To delineate the molecular basis
121 for how Calcineurin binds to PI4KA we examined the architecture using an approach
122 combining cryo-EM, HDX-MS, and AlphaFold3 modelling.

123 We first conducted cryo-EM analysis of the PI4KA complex bound to Calcineurin.
124 Although negative stain analysis revealed that the purified PI4KA complex bound to
125 Calcineurin was homogeneous, our initial attempts to obtain good 3D reconstructions
126 were unsuccessful due to preferred particle orientation. We reasoned that this could likely
127 be due to the dynamic nature of Calcineurin relative to PI4KA, and PI4KA's proposed
128 membrane binding interface leading to the accumulation of PI4KA at the air-water
129 interface. To obtain a more "rigid" complex for cryo-EM analysis, we treated the PI4KA
130 complex bound to Calcineurin with BS^3 crosslinker, followed by gel filtration to remove
131 aggregate proteins. The crosslinked complex eluted from gel filtration equivalently to the
132 non-crosslinked complex. Analysis of this complex allowed for the refinement of 235,760
133 particles leading to a 3D reconstruction at a nominal resolution of 3.50 Å (Fig 1C, Fig S1).

134 The density map was of sufficient quality to allow for automated and manual
135 building of the majority of the PI4KA subunit, with a clear orientation of the available cryo-
136 EM and X-ray crystallography models of TTC7B-FAM126A in the electron density,
137 although we had only weak density for the N-terminal region of TTC7B therefore we
138 removed this from our molecular model. [10,16]. The regions with the lowest local resolution
139 correspond to the two Calcineurin molecules. Despite this, the low local resolution of the
140 map for Calcineurin (~7 Å) was sufficient to allow for a rigid body fit of previously solved
141 high resolution Calcineurin structures into the density, and allowed for an orientation of
142 Calcineurin relative to PI4KA. However, at this resolution we could not experimentally
143 define the residues mediating the interaction between PI4KA and Calcineurin, and this

144 interface was predicted using AlphaFold3, and validated using HDX-MS (described
145 below).

146 Our cryo-EM map captures more details in PI4KA than compared to the previously
147 reported cryo-EM structure of the PI4KA complex [10]. While the interface between TTC7
148 and PI4KA in the dimerization and helical domains of PI4KA have been extensively
149 characterised [10], the interaction between the solenoid domain of PI4KA and Calcineurin
150 have been structurally unresolved. Using a combination of manual model building and
151 AlphaFold/trRosetta modelling of specific regions [24,25] we were able to confidently build
152 an additional ~700 residues of PI4KA corresponding to the solenoid α helices in the horn
153 domain (Fig S2 and S3). Intriguingly, the solenoid horn domain showed a slight deviation
154 compared to the previous cryo-EM structure of PI4KA (Fig S2B). It is not known if this
155 conformational difference was driven by the interaction with Calcineurin or by the
156 chemical crosslinker used to stabilize the assembly. The local resolution of the contact
157 between the N-terminus of PI4KA and TTC7B allowed for unambiguous determination of
158 the residues mediating this interface (Fig 2, S1C, S2C). The interface between the N-
159 terminus of the horn domain (composed of solenoid α helices 1+2 [residues 31-59], Fig
160 2C) and the C-terminus of TTC7B was evolutionarily conserved through *C. elegans* (Fig
161 2D), while only weakly conserved in yeast. It has been previously shown that disease-
162 linked C-terminal truncations in TTC7A that disrupt this interface can still bind to PI4KA,
163 although they show decreased PI4KA activity [10]. Studies on PI4KA were initially
164 complicated by improper annotation of the N-terminal start site (ORF starting at M59) [15],
165 with our results revealing the molecular basis for why the two evolutionarily conserved N-
166 terminal PI4KA helices immediately before this site are critical in mediating contact with
167 the C-terminus of TTC7. This further reinforces that any cellular studies examining
168 PI4KA's roles with a construct containing the improperly annotated start site should be
169 interpreted with extreme caution.

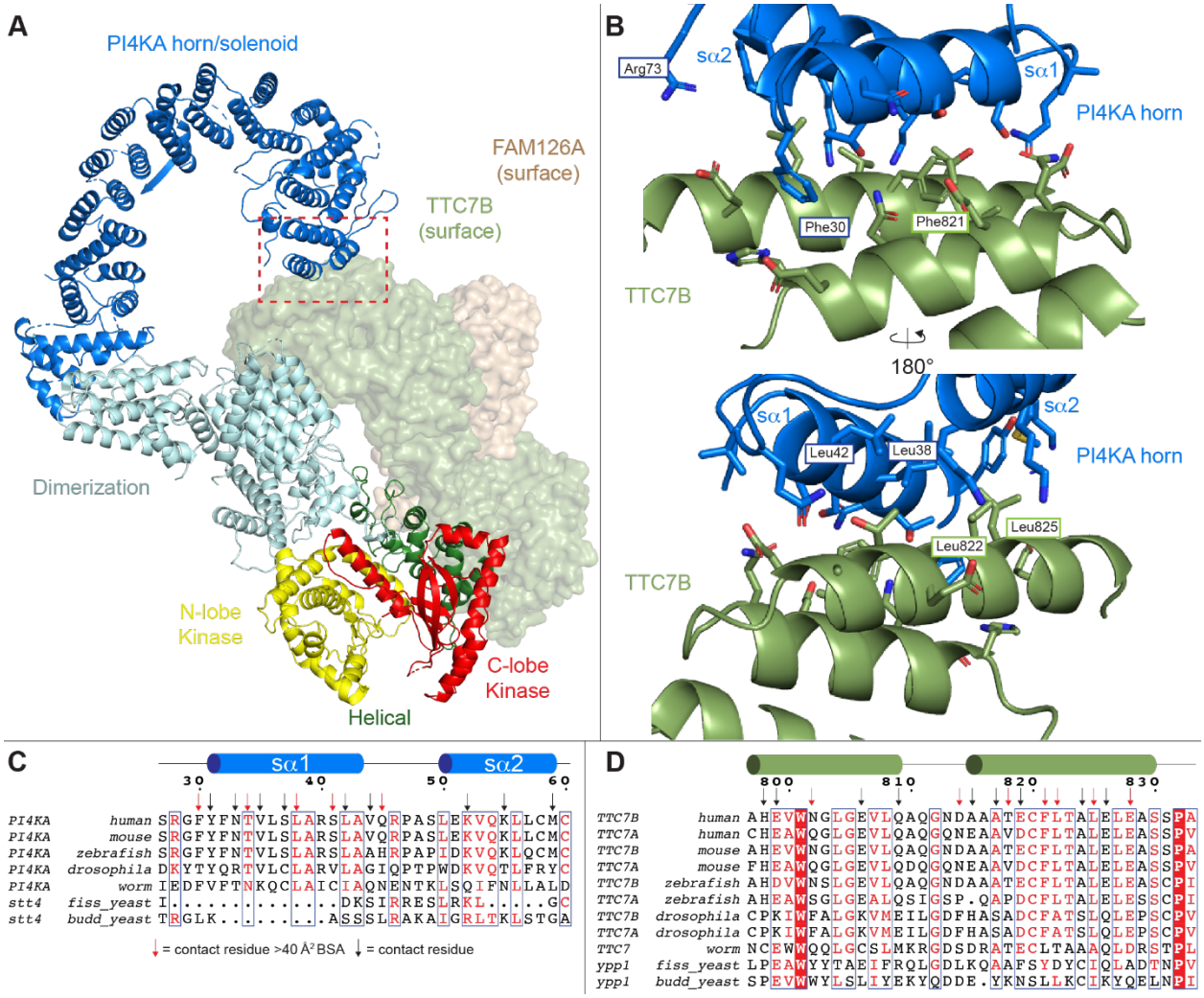

Figure 2. The N-terminus of the PI4KA solenoid interacts with the TTC7B C-terminal region

A. Cartoon representation of an isolated PI4KA/TTC7B/FAM126A trimer. PI4KA is shown as a cartoon with individual domains coloured according to the in-figure text. TTC7B and FAM126A are shown as surfaces coloured according to the in-figure text. Red box depicts the PI4KA solenoid-TTC7B interface.

B. Cartoon representation of the PI4KA solenoid-TTC7B interaction interface. Side chains are shown for residues within 6 Å of either interface, which are either annotated on the cartoon or in panel C/D. Annotated residues on the cartoon were chosen to provide readers with a point of reference.

C. Multiple sequence alignment of PI4KA from *Homo sapiens, Mus musculus, Danio rerio, Drosophila melanogaster, Caenorhabditis elegans*, *Schizosaccharomyces pombe,* and *Saccharomyces cerevisiae.* sα1 and sα2 are annotated above the alignment. Residues within 6 Å shown in panel B are annotated using arrows, with red arrows indicating a BSA of > 40 Å^2.

D. Multiple sequence alignment of TTC7A/B from *Homo sapiens, Mus musculus, Danio rerio, Drosophila melanogaster, Caenorhabditis elegans*, *Schizosaccharomyces pombe,* and *Saccharomyces cerevisiae.* TTC7B secondary structure observed from experimental data is annotated above the alignment. Residues within 6 Å shown in panel B are annotated using arrows, with red arrows indicating a BSA of > 40 Å^2.

186

187 **Cryo-EM, AlphaFold3, and HDX-MS analysis of PI4KA-Calcineurin binding site**

188 The local resolution of Calcineurin allowed us to fit previously solved structures of
189 Calcineurin into the density [26], however, it was not sufficient to model the exact PI4KA
190 residues mediating binding. To precisely map the location of the Calcineurin binding site
191 we utilised AlphaFold3 to predict the interface, and HDX-MS, which is a technique for
192 probing protein dynamics and characterizing protein-protein interfaces [27–29] to validate
193 the prediction.

194 Having experimentally identified a binding event between Calcineurin and PI4KA,
195 we carried out AlphaFold3 analysis to predict the interface responsible for this interaction
196 [30]. We carried out searches composed of Calcineurin (CNA alpha 1 (2-391) and CNB)
197 along with our PI4KA complex construct (PI4KA/TTC7B/FAM126A 1-308). The resulting
198 prediction had overall ptm and iptm scores of 0.76 and 0.74, respectively, consistent with
199 a confident multi-protein prediction (see methods). AlphaFold3 predicted with high
200 confidence a beta strand (residues 536-541 containing the IKISVT sequence) in PI4KA
201 binding to the NIR region of Calcineurin that mediates binding to PxIxIT motifs, with
202 predicted alignment error (PAE) scores consistent with a stable interface (Fig. 3A/B/C).
203 We also observed that an unstructured loop in PI4KA's dimerization domain formed an
204 interaction with CNB at the LxVP SLiM motif binding pocket, however, with lower pLDDT
205 and PAE scores compared to the PI4KA-CNA interface. There were no other predicted
206 interactions between PI4KA and Calcineurin. The AlphaFold3 prediction fit well into our
207 low-resolution cryo-EM map after rigid body refinement.

208

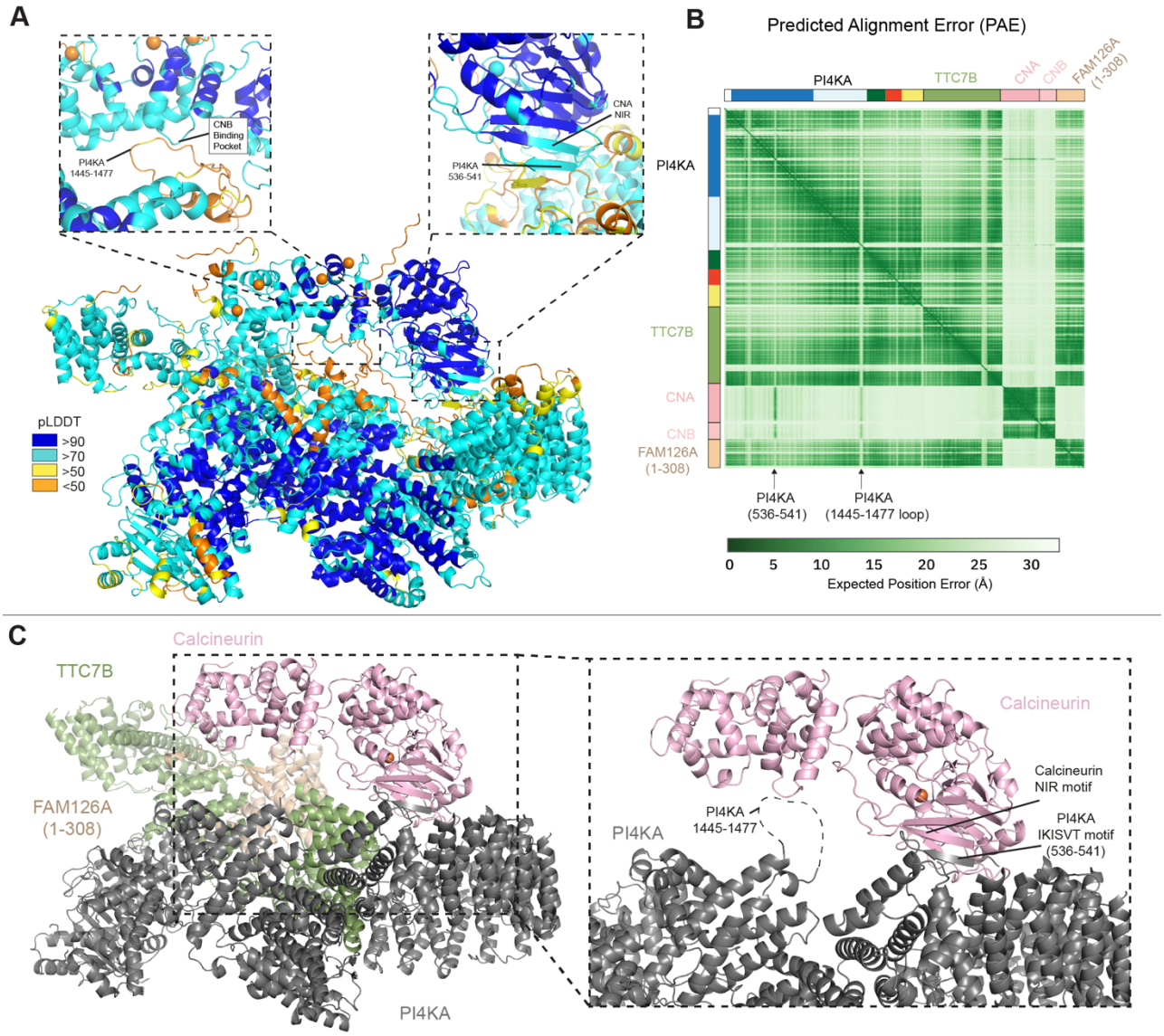

Figure 3. AlphaFold3 predicts a dual interface between PI4KA and Calcineurin

A. AlphaFold3 prediction of PI4KA/TTC7B/FAM126A ΔC in complex with Calcineurin and co-factors with the per-residue confidence metric predicted local-distance difference test shown as per the legend, with zoom-ins of the predicted PI4KA interface with (L) the Calcineurin B LxVP binding pocket and (R) Calcineurin A NIR motif.

B. Predicted aligned error (PAE) of the AlphaFold3 prediction of the PI4KA/TTC7B/FAM126A (1-308) in complex with Calcineurin and co-factors.

C. AlphaFold3 prediction of PI4KA/TTC7B/FAM126A ΔC in complex with Calcineurin and co-factors, with pLDDT <60 removed. (R) Zoom in on the predicted PI4KA – Calcineurin interface, with TTC7B and FAM126A ΔC removed. Dotted grey line represents region with a low pLDDT score.

221 To validate the AlphaFold3 prediction, HDX-MS experiments were conducted. The
222 rate at which deuterium is exchanged on the amide backbone is dependent on the stability
223 of protein secondary structure. Deuterium incorporation is localised at peptide-level
224 resolution through the generation of pepsin-generated peptides, therefore allowing us to
225 map the protein-protein interface at peptide level resolution. HDX experiments compared
226 the dynamics of Calcineurin and the PI4KA complex both free in solution and when in the
227 co-complex. Initial experiments were carried out at a high concentration of PI4KA complex
228 and Calcineurin (1.3 μM final) at a 1:1 ratio complex, with deuterium incorporation
229 measured over three time points (3, 30, 300 s at 18°C at pH 7.0). These experiments
230 were carried out under three conditions: Calcineurin apo, PI4KA complex apo, and the
231 co-complex, allowing us to map changes on both sides of the interface. These
232 experiments revealed that the interacting motifs in PI4KA were all in regions that were
233 disordered [23], consistent with the biophysical properties of the motifs that mediate
234 interaction(s) with Calcineurin [31,32]. To better cover the deuterium incorporation of these
235 highly dynamic regions we carried out an additional experiment using a pH and
236 temperature regime optimized for disordered regions (pH 6.5, 0°C) [33]. Experiments were
237 carried out with a 1:2 ratio of the PI4KA complex to Calcineurin (1.25 and 2.5 μM final),
238 with deuterium incorporation measured over three time points (3, 10, 30 s). The full raw
239 deuterium incorporation data for all HDX-MS experiments are provided in the source data.
240 Coverage of all proteins was over 85%, with all HDX-MS processing statistics available
241 in the source data.

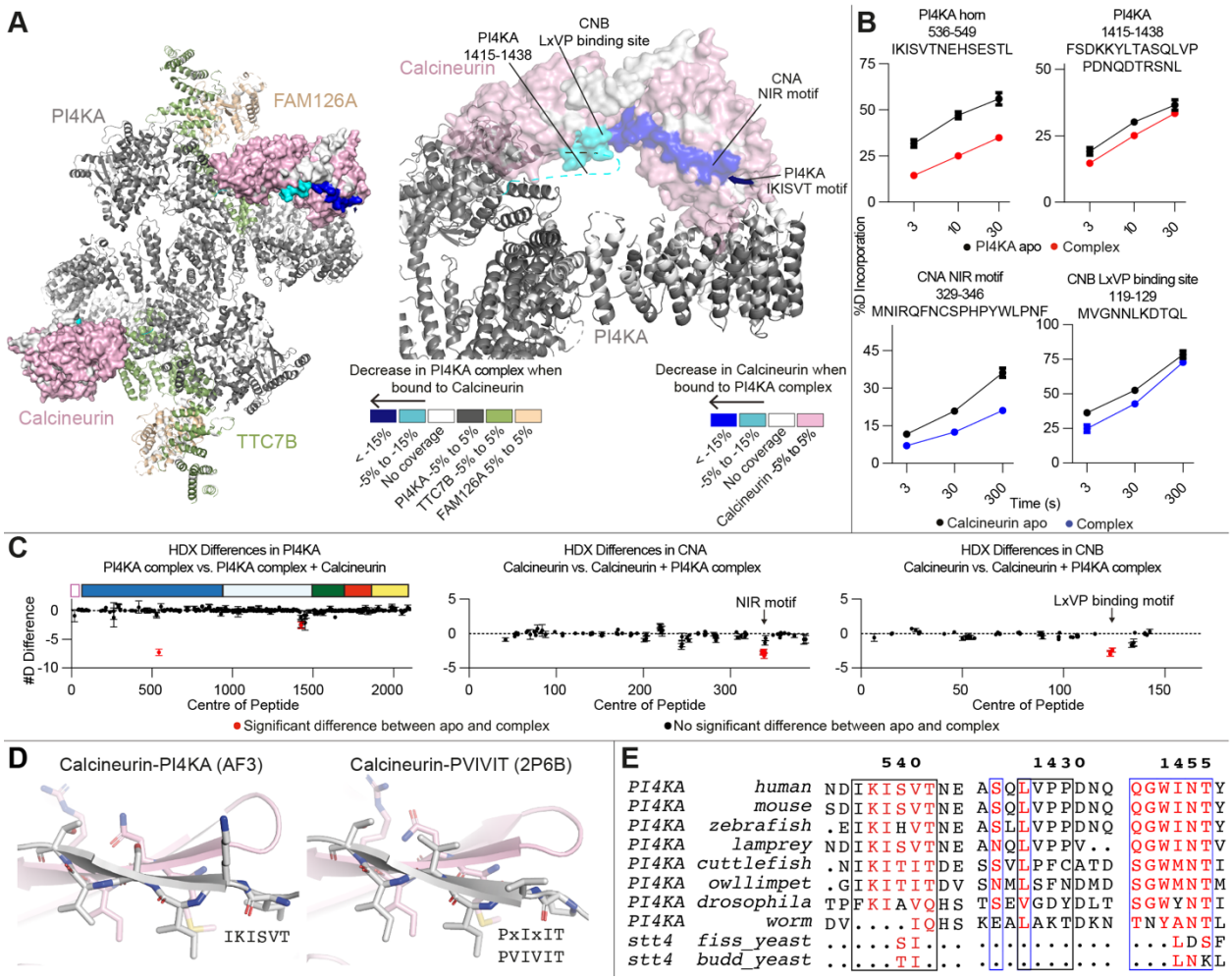

Figure 4. Calcineurin interacts with the PI4KA solenoid

A. (L) PI4KA complex (pH 6.5, 0°C) and Calcineurin (pH 7.0, 18°C) peptides showing significant differences in deuterium exchange (defined as >5%, 0.45 Da, and p<0.01 in an unpaired two-tailed t test at any time point) upon complex formation. Differences are mapped on the structural model, with a disordered loop showing changes in HDX being represented by a dotted line. Differences are indicated by the legend. (R) Differences are mapped on a zoomed in structural model of the interface. Differences are indicated by the legend in A.

B. Selected deuterium exchange time courses of PI4KA (pH 6.5, 0°C) and Calcineurin (pH 7.0, 18°C) peptides that showed significant decreases in exchange upon complex formation. Error is shown as standard deviation (SD) (n=3).

C. Sum of the number of deuteron difference of (L) PI4KA upon complex formation with Calcineurin (pH 6.5, 0°C), (M) Calcineurin A or (R) Calcineurin B upon complex formation with the PI4KA complex (pH 7.0,18°C), analysed over the entire deuterium exchange time course for PI4KA complex/Calcineurin. (M/R) Each point is representative of the centre residue of an individual peptide. Peptides that met the significance

257 criteria described in panel D are coloured red. Error is shown as the sum of standard deviations across all
258 3 time points (SD) (n=3).
259 **D.** Cartoon representation of the (L) IKISVT mediated interaction with Calcineurin's NIR motif and (R)
260 canonical PxIxIT mediated interaction with Calcineurin's NIR motif.
261 **E.** Multiple sequence alignment of PI4KA from *Homo sapiens, Mus musculus, Danio rerio, Petromyzon*
262 *marinus, Sepia pharaonis, Lottia gigantea, Drosophila melanogaster, Caenorhabditis elegans*,
263 *Schizosaccharomyces pombe,* and *Saccharomyces cerevisiae,* showing conservation of the PI4KA IKISVT
264 motif, and regions of the PI4KA dimerization domain unstructured loop.
265
266 We observed a significant decrease (significant change defined as greater than
267 both 5% and 0.45 Da at any time point in any peptide with an unpaired two-tailed t test
268 $p<0.01$) in deuterium exchange at residues 331-347 (NIR binding site) in CNA, residues
269 119-129 (LxVP binding pocket) in CNB, and residues 538-549 and 1417-1438 in PI4KA.
270 The 538-549 region is an unstructured region between solenoid α helices 17 and 18 (Fig
271 4A-C, S4). This is similar to decreases in exchange observed when using full length
272 PI4KA complex [23], however the absence of the FAM126A C-terminus allows for a
273 confident validation of a protein-protein interface. The additional decrease in exchange
274 was observed in PI4KA at residues 1417-1438, which covers an unstructured region
275 containing sequence previously observed to bind CNB [34].
276 We conducted multiple sequence alignments of PI4KA to identify conserved
277 elements that may mediate binding. We found that the IKISVT binding site for Calcineurin
278 in PI4KA and the potential LVPP binding site showing decreased exchange by HDX-MS
279 were evolutionarily conserved throughout all vertebrates, with them being partially
280 conserved in chordates, and lost in arthropods (Fig. 4E). However, we found that an
281 additional WINT motif in the unstructured 1427-1477 loop was also evolutionarily
282 conserved throughout all chordates and lost in arthropods (Figure 4E), with this binding
283 site being predicted by AlphaFold3. The binding of IKISVT bound to the NIR region of
284 Calcineurin is consistent with Calcineurin binding to the canonical PxIxIT docking groove
285 (Fig. 4D), and is also consistent with the high degree of plasticity observed in Calcineurin
286 SLiM motifs [31,32]. To fully understand the role of either the LVPP or WINT sequences in

287 the 1427-1477 PI4KA loop binding to CNB's LxVP binding pocket, further experiments
288 will be required.
289
290 **Comparison of the FAM126A-Calcineurin and PI4KA-Calcineurin binding sites**
291 To fully understand the myriad molecular interactions mediating how the PI4KA
292 complex interacts with Calcineurin, we wanted to determine how the C-terminus of
293 FAM126A, which is absent from our cryo-EM structure, might interact with Calcineurin.
294 To investigate this interaction, we purified the FAM126A C-terminus [FAM126A (415-
295 521)] and used HDX-MS to compare the dynamics of FAM126A (415-521) apo to
296 FAM126A (415-521) in complex with Calcineurin (Fig. 5, S4). The full raw deuterium
297 incorporation data for all HDX-MS experiments are provided in the Source Data.
298 The HDX-MS experiments were carried out at a 1:1 ratio, with deuterium
299 incorporation measured over three time points (3, 30, 300 s at 0°C). As the C-terminus of
300 FAM126A is intrinsically disordered in the absence of binding partners (Fig 5A), we
301 carried out HDX-MS experiments at a temperature of 0°C and a pH of 6.5 to optimize the
302 experiment for rapidly exchanging amide hydrogens [33]. Two areas in FAM126A (415-521)
303 had significant changes in deuterium exchange upon complex formation with Calcineurin
304 (significant change defined as greater than both 5% and 0.45 Da at any time point in any
305 peptide with an unpaired two-tailed t test $p<0.01$). As expected, the largest significant
306 decrease in deuterium exchange occurred in peptides containing the PSISIT binding site
307 (494-521) (Fig. 5D-F). Another site with a significant decrease in deuterium contained an
308 LTLT sequence (423-450), which we postulated may be able to bind in the LxVP binding
309 pocket [35]. Alphafold3 was used to predict the structure of the FAM126A-mediated
310 interaction of PI4KA and Calcineurin (Fig. 5B-C) [30], with the LTLT (426-429) and PSISIT
311 (512-517) sequences predicted to bind in the LxVP and PxIxIT binding sites on
312 Calcineurin, with predicted alignment error indicative of a stable interface.

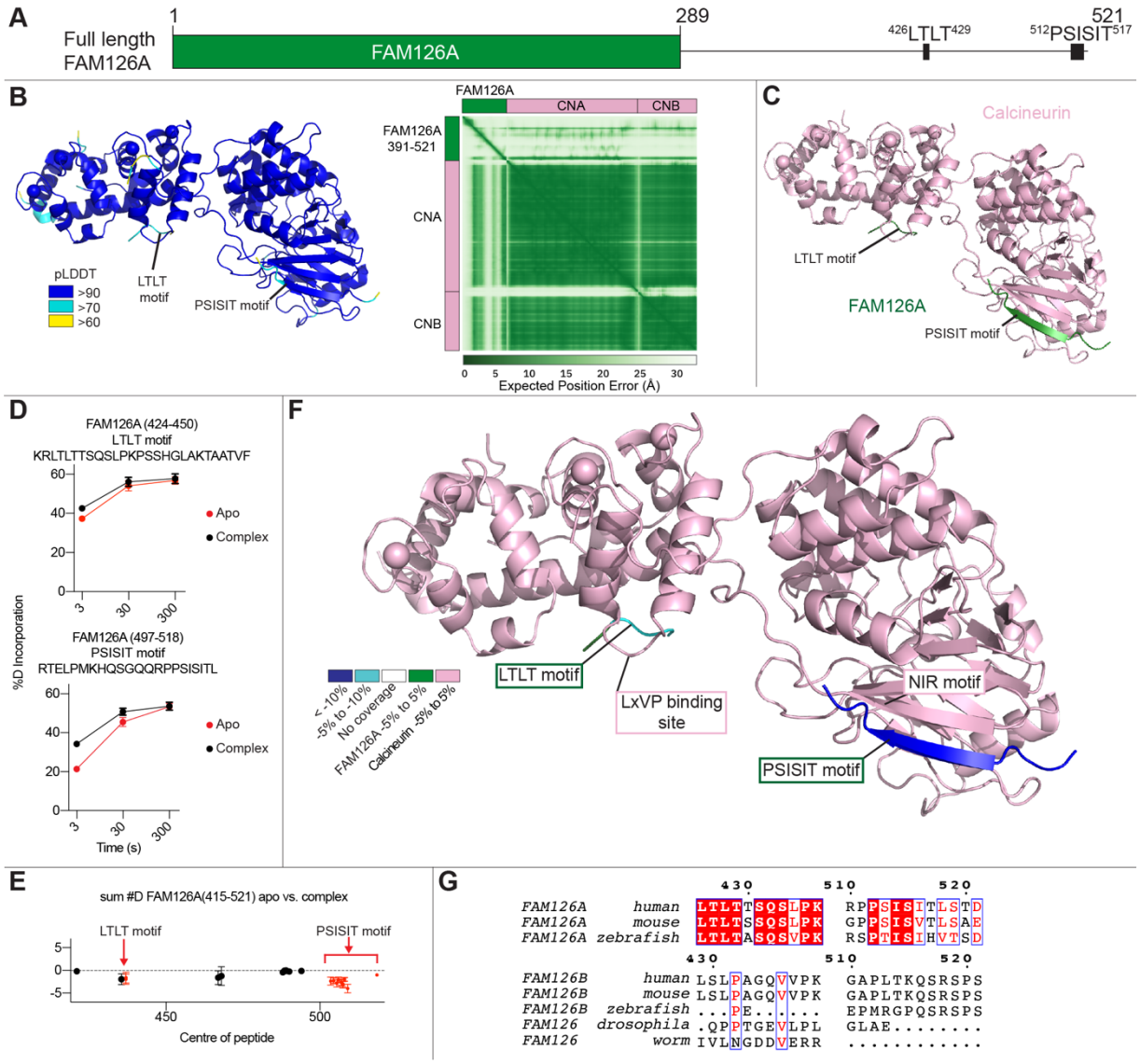

Figure 4. FAM126A LTLT motif interacts with CNB's LxVP binding site

A. Domain schematic of FAM126A highlighting the disordered C-terminal which contains conserved LTLT and PSISIT motifs.

B. (L) AlphaFold3 prediction of Calcineurin in complex with the FAM126A C-terminal tail coloured with the per-residue confidence metric predicted local-distance difference test (pLDDT) as per the legend, and pLDDT <60 removed. (R) Predicted aligned error (PAE) of the AlphaFold3 search of Calcineurin and the FAM126A C-terminal tail.

C. AlphaFold3 prediction of Calcineurin in complex with the FAM126A C-terminal tail with pLDDT <60 removed. Domains are coloured according to the in-figure text.

D. Selected deuterium exchange time courses of FAM126A (415-521) and Calcineurin peptides that showed significant (defined as >5% 0.45 Da, and p<0.01 in an unpaired two-tailed t test at any time point) decreases in exchange. Error is shown as standard deviation (SD) (n=3).

326 **E.** Sum of the number of deuteron difference of FAM126A (415-521) upon complex formation with
327 Calcineurin analysed over the entire deuterium exchange time course for FAM126A (415-521). Each point
328 is representative of the centre residue of an individual peptide. Peptides that met the significance criteria
329 described in F are coloured red. Error is shown as the sum of standard deviations across all 3 time points
330 (SD) (n=3).
331 **F.** Peptides showing significant differences in deuterium exchange upon complex formation. Differences
332 are mapped on the AlphaFold3 prediction shown in panel C. Differences are indicated by the legend.
333 **G.** Multiple sequence alignment of FAM126A (from *Homo sapiens, Mus musculus,* and *Danio rerio*) and
334 FAM126B/FAM126 (from *Homo sapiens, Mus musculus, Danio rerio, Drosophila melanogaster,* and
335 *Caenorhabditis elegans*.
336

337 **Discussion**

338 We had previously discovered that PI4KA was regulated by the plasma membrane
339 localised CNAβ1 isoform of Calcineurin, with Calcineurin playing a role in regulating PI4P
340 synthesis at the plasma membrane downstream of GPCR signaling [23]. In this study, we
341 aimed to investigate the full complement of molecular mechanisms underlying this
342 regulatory role of Calcineurin in PI4KA signaling. Our synergistic application of cryo-EM,
343 HDX-MS, and AlphaFold3 modelling has established that the PI4KA complex contains
344 two proteins that have evolutionarily conserved and distinct Calcineurin binding sites.
345 PI4KA has two regions that bind Calcineurin, one located in the horn domain, and one in
346 the dimerization domain, with FAM126A binding to Calcineurin through its disordered C-
347 terminus.

348 An important question posed from this work, is the evolutionary mechanism
349 explaining why PI4KA has some of the largest variations in Calcineurin binding SLiM
350 motifs [31,32]. This could be driven by CNAβ1 being the only Calcineurin isoform to be
351 directly localised to the plasma membrane through palmitoylation with it being at a higher
352 local concentration relative to PI4KA compared to other calcineurin substrates through
353 membrane co-localization [23]. However, variation from the canonical LxVP and PxIxIT
354 motifs in Calcineurin regulated proteins has been observed, including Calcineurin binding
355 proteins containing IAIIIT [36] and LVPP sequences at their binding sites [34]. Another
356 important unanswered question of our work is why the PI4KA complex has evolved to

357 have Calcineurin binding sites on both FAM126A and PI4KA. This is especially puzzling
358 as PI4KA can bind either FAM126A or FAM126B, with only FAM126A containing a SLiM
359 motif. Further cellular and organismal analysis of mutants in both the PI4KA and
360 FAM126A sites will be required to understand their precise role in PI4KA signaling, and
361 any FAM126A-specific functions in Calcineurin/PI4KA signaling.

362 Canonically, Calcineurin binds to substrate SLiM motifs to orient substrate
363 phosphorylation sites towards the phosphatase active site of Calcineurin [22,31,32]. We
364 previously identified a CNAβ1 regulated phosphosite in the C-terminus of FAM126A [23],
365 which suggested that there likely could be additional phosphorylation sites in the vicinity
366 of the PI4KA horn site. There is an annotated phosphorylation site at S1436 near a region
367 with decreased deuterium exchange in PI4KA, which could be dephosphorylated by
368 Calcineurin. There are also extensive phosphorylation sites present in the C-terminus of
369 both TTC7A and TTC7B that are in close spatial proximity to Calcineurin (Fig. S5A-C) [37].
370 These sites are present in a disordered loop (642-703 in TTC7B, and 650-688 in TTC7A)
371 that could be accessible to the active site of Calcineurin when comparing AlphaFold
372 models of these loops to our cryo-EM structure (Fig. S5B-D). Intriguingly, this loop is in
373 direct proximity to the proposed binding site for EFR3, which recruits PI4KA to the plasma
374 membrane [12]. In yeast, phosphorylation of Efr3 downregulates PI4KA recruitment through
375 decreased association with the TTC7 isoform Ypp1 [16]. Further experimentation defining
376 the binding interface of EFR3 to the PI4KA complex should consider the possible role of
377 these PTMs in TTC7 in regulating PI4KA membrane localisation and activity.

378 A important aspect in the regulation of almost all phosphoinositide kinases is their
379 recruitment to membrane surfaces, with this mediated by multiple mechanisms, including
380 protein-protein and protein-lipid interactions, as well as post-translational modifications
381 [38–40]. PI4KA is primarily active at the PM [15], with the CNAβ1 isoform of Calcineurin also
382 being localised at the PM through palmitoylation [23]. A limitation of our study is that we are
383 studying the association of the PI4KA complex with Calcineurin in solution, and not in the
384 biologically relevant context of the plasma membrane. There are technical challenges
385 associated with studying a large peripheral membrane protein complex by cryo-EM and
386 HDX-MS approaches. However, the insights gained from this work are relevant, as the

387 presence of a membrane will likely only enhance complex formation due to increased
388 local concentration but not alter the mode of interaction observed in our studies.
389 Nevertheless, future studies should focus on delineating the role of PI4KA-Calcineurin
390 interface in cellular membranes.

391 Overall, our work reveals important new insight into the molecular basis for how
392 CNAβ1 can bind to and regulate the PI4KA complex. The structural insight generated by
393 our work provides an exciting platform for continued investigations into how
394 phosphorylation regulates PI4KA, and how calcium signaling is integrated into PI4P
395 production at the plasma membrane.

396

397 **STAR Methods**

398 **Key Resources Table**

REAGENT or RESOURCE	SOURCE	IDENTIFIER
Bacterial and virus strains		
E.coli DH10EMBacY Competent Cells	Geneva Biotech	DH10EMBacY
E.coli C41(DE3) chemically competent cells	Lab stock	
Chemicals, peptides, and recombinant proteins		
Deuterium Oxide 99.9%	Sigma Aldrich	151882-10X1ML
BS^3	Thermo Scientific	21580
Deposited Data		
Mass spectrometry proteomics data	This paper	PXD043409 PXD050633
PDB	This paper	9B9G
EMDB	This paper	44382
Recombinant DNA		
PI4KA complex PI4KA/TTC7B/FAM126A (1-308)	Dornan et al., 2018	GD177
Calcineurin-GST expression vector	Ulengen-Talkish et al., 2021	Calcineurin
Calcineurin strep-his expression vector	This paper	AS27
MBP-FAM126A (415-521)	This paper	AS39
Software and algorithms		
cryoSPARC v4.2.1	Structura Bio	https://cryosparc.com
Phenix-1.19.1	Open source	https://phenix-online.org/
COOT-0.9.4.1	CCP4	https://www2.mrc-lmb.cam.ac.uk/personal/pemsley/coot/

HDExaminer	Sierra Analytics	http://massspec.com/hdexaminer
Bruker Compass DataAnalysis 4.2	Bruker	www.bruker.com
GraphPad Prism 7	GraphPad	https://www.graphpad.com
PEAKS 7	Bioinformatics Solutions Inc.	https://www.bioinfor.com/versions/
FragPipe (v19.1)	Nesvizhskii Lab- University of Michigan	fragpipe.nesvilab.org
Adobe Illustrator	Adobe	https://www.adobe.com/products/illustrator.html
ESPript 3.0	SBGrid consortium	https:espript.ibcp.fr
PyMOL	Schroedinger	http://pymol.org
Other		
C-flat Holey Thick Carbon Grid 2.0 μm hole 1.0 μm space 300 mesh	Electron Microscopy Studies	CFT312-100
SF9 insect cells for expression	Expression Systems	94-001S
Affipro pepsin column, 69.3 μL, 2.1 mm X 20 mm	Affipro	AP-PC-001
ProDx Pepsin Column F 10-32	Trajan Scientific Americas	PDX.PP01-F32
ACQUITY UPLC Peptide BEH C18 Column, 300Å, 1.7 μm, 2.1 mm X 100 mm, 1K – 30K	Waters	186003686
ACQUITY UPLC BEH C18 1.7 μm, 2.1 mm x 5 mm	Waters	186004629

Resource availability

Lead contact

Further information and requests for resources and reagents should be directed to and will be fulfilled by the lead contact John E Burke (jeburke@uvic.ca)

Materials availability

All materials generated from this study will be available by request to the lead contact.

413 **Experimental model and subject details**

414 PI4KA complex was expressed in *Spodoptera frugiperda* (Sf9) cells. Sf9 cells (94-001S)
415 were obtained from Expression Systems (CA, USA) and were cultured ESF 921 media
416 (96-001-01, Expression Systems, CA, USA) at 27°C. Calcineurin and the MBP-FAM126A
417 construct were expressed in C41 (DE3) *E.coli* in 2xYT media.

418

419 **Method Details**

420 ***Multiple Sequence Alignments***

421 Multiple sequence alignments were generated using Clustal Omega. Aligned sequences
422 were then analysed by ESPript 3.0 (https://espript.ibcp.fr) [41] to visualize conservation.
423 The uniprot accession codes for Figure 2C are P42356, E9Q3L2, A0A8M3AWF4,
424 Q9W4X4, Q9XW63, Q9USR3, and P37297. The uniprot accession codes for Figure 2D
425 are Q86TV6, Q9ULT0, E9Q6P5, Q8BGB2, A1L101, A0A8M9QA29, A0A0B4K7H0,
426 Q7KN74, H2KYB6, O94441, and P46951. The uniprot accession codes for Figure 3G are
427 P42356, E9Q3L2, Q49GP4, S4RUP9, ASA812BZT7, V4C7L9, Q9W4X4, Q9XW63,
428 Q9USR3, and P37297. The uniprot accession codes for Figure 4G are Q9BYI3, Q6P9N1,
429 Q6P121, Q8IXS8, Q8C729, A1A5W7, Q7K1C5, and Q6A586.

430

431 ***Protein Expression***

432 PI4KA complex (PI4KA/TTC7B full length, FAM126A (1-308)) was expressed from
433 bacmids harbouring MultiBac constructs which were transfected into *Spodoptera*
434 *frugiperda (Sf9) cells,* and viral stocks amplified for one generation to acquire a P2
435 generation viral stock. Final viral stocks were added to *Sf9 cells* in a 1/100 virus volume-
436 to-cell ratio. Constructs were expressed for 65-72 hours before pelleting of infected cells.
437 GST-tagged or SII-10xHis (2x strep with 10x his) human calcineurin A (aa 2-391 human
438 CNA alpha isoform) in tandem with calcineurin B were expressed in BL21 C41
439 *Escherichia coli*, induced with 0.1 mM IPTG (isopropyl β-d-1-thiogalactopyranoside) and
440 grown at 23°C overnight. SII-10xHis MBP tagged FAM126A (415-521) was expressed in
441 BL21 C41 *Escherichia coli* induced with 0.5 mM IPTG and grown at 37°C for 3 hours. Cell

442 pellets were washed with PBS immediately prior to being snap-frozen in liquid nitrogen,
443 then stored at -80°C.
444
445 ***Protein purification***
446 For PI4KA complex purification, *Sf9* pellets were re-suspended in lysis buffer [100 mM
447 NaCl, 20 mM imidazole (pH 8.0), 5% glycerol (v/v), 2 mM βMe, protease inhibitor
448 (Protease Inhibitor Cocktail Set III, EDTA-Free)] and lysed by sonication for 2.5 minutes.
449 Triton X-100 was added to a 0.1% (v/v) and centrifuged for 45 minutes at 20,000 g at 1°C
450 (Beckman Coulter J2-21, JA 20 rotor). The supernatant was loaded onto a 5 ml HisTrap
451 FF Crude column (Cytiva), washed with NiNTA A buffer [100mM NaCl, 20 mM imidazole
452 (pH 8.0), 5% glycerol (v/v), 2 mM βMe], washed with 10% NiNTA B buffer, and eluted
453 with NiNTA B buffer [100 mM NaCl, 450 mM imidazole (pH 8.0), 5% glycerol (v/v), 2 mM
454 βMe]. The eluent was loaded onto a 5 mL StrepTrap column (Cytiva) pre-equilibrated with
455 GFB [150 mM NaCl, 20 mM imidazole (pH 7.0), 5% glycerol (v/v), 0.5 mM TCEP] then
456 washed prior to the addition of a lipoyl domain containing TEV protease. TEV cleavage
457 proceeded overnight before elution with 10 mL of GFB. Protein was concentrated using
458 an Amicon 50 kDa MWCO concentrator (MilliporeSigma). PI4KA complex used for
459 crosslinking experiments with Calcineurin was taken after this concentration step (see
460 below, *Crosslinking*). PI4KA complex used for HDX-MS experiments was loaded onto a
461 pre-equilibrated [150 mM NaCl, 20 mM imidazole (pH 7.0), 5% glycerol (v/v), 0.5 mM
462 TCEP] Superose 6 Increase column (Cytiva) and protein-containing fractions were
463 collected, concentrated, flash frozen in liquid nitrogen, and stored at -80 °C. The
464 stoichiometry of the PI4KA based on size exclusion chromatography, SDS-PAGE, and
465 negative stain microscopy is equimolar (2:2:2).
466 *Escherichia coli* cell pellets containing GST-tagged human Calcineurin were lysed
467 by sonication for 5 minutes in lysis buffer [50 mM Tris (pH 8.0), 100 mM NaCl, 2 mM
468 EDTA, 2 mM EGTA, protease inhibitors (Millipore Protease Inhibitor Cocktail Set III,
469 Animal-Free)]. NaCl was then added to 1 M and the lysed solution was centrifuged at
470 20,000 g at 1°C for 45 minutes (Beckman Coulter J2-21, JA 20 rotor). Tween-20 was
471 added to the supernatant to 0.1% (v/v) then loaded onto a 5 mL GSTrap 4B column

472 (Cytiva) in a super loop fashion for 1 hour, then washed in Wash Buffer [50 mM Tris (pH
473 8.0), 110 mM KOAc, 2 mM MgOAc, 0.02% CHAPS (w/v), 5% glycerol (v/v) 0.5 mM TCEP]
474 to remove non-specifically bound protein. To remove GroEL chaperone the column was
475 washed with Wash buffer containing 2 mM ATP. To remove the GST tag, PreScission
476 protease was added to the column and incubated overnight at 4°C. The cleaved protein
477 was eluted with 7 mL of Wash Buffer. The eluant underwent size exclusion
478 chromatography (SEC) using a Superdex 200 10/300 column (Cytiva) equilibrated in GFB
479 [150 mM NaCl, 20 mM imidazole (pH 7.0), 5% glycerol (v/v), 0.5 mM TCEP] for
480 crosslinking experiments, or Wash Buffer [50 mM Tris (pH 8.0), 110 mM KOAc, 2 mM
481 MgOAc, 0.02% CHAPS (w/v), 5% glycerol (v/v) 0.5 mM TCEP]. For crosslinking reaction
482 (see below, *Crosslinking*), fresh, concentrated protein was used. In all other cases,
483 fraction(s) containing protein of interest were pooled, concentrated, flash frozen in liquid
484 nitrogen and stored at -80°C.

485 *Escherichia coli* cell pellets containing SII-10xHis tagged Calcineurin were lysed
486 by sonication for 5 minutes in lysis buffer (50 mM Tris pH 8.0 (RT), 100 mM NaCl, 2 mM
487 EDTA, 2 mM EGTA, 10 mM Imidazole pH 8.0 (RT), 2 mM βMe, protease inhibitors
488 (Millipore Protease Inhibitor Cocktail Set III, Animal-Free)). NaCl was added to 1 M and
489 the lysed solution was centrifuged at 20,000 g for 50 minutes at 4°C. Tween-20 was
490 added to the supernatant to 0.1% (v/v) then loaded onto a HisTrap FF Crude column
491 (Cytiva), washed with NiNTA A buffer [50 mM Tris pH 8.0 (RT), 100 mM NaCl, 2 mM
492 EDTA, 2 mM EGTA, 10 mM Imidazole pH 8.0 (RT),2 mM βMe], washed with 6% NiNTA
493 B buffer, and eluted with NiNTA B buffer [50 mM Tris pH 8.0 (RT), 100 mM NaCl, 2 mM
494 EDTA, 2 mM EGTA, 200 mM Imidazole pH 8.0 (RT),2 mM βMe]. The eluent was loaded
495 onto a 5 mL StrepTrap column pre-equilibrated with GFB [20 mM HEPES (pH 7.5) RT,
496 150 mM NaCl, 0.5 mM TCEP] then washed prior to the addition of a lipoyl domain
497 containing TEV protease. TEV cleavage proceeded overnight before elution with 12 mL
498 of GFB. The eluant underwent size exclusion chromatography (SEC) using a Superdex
499 200 10/300 column equilibrated in GFB [150 mM NaCl, 20 mM imidazole (pH 7.0), 5%
500 glycerol (v/v), 0.5 mM TCEP]. Fraction(s) containing protein of interest were pooled,
501 concentrated, flash frozen in liquid nitrogen and stored at -80°C

502 *Escherichia coli* cell pellets containing FAM126A (415-521) were lysed by
503 sonication for 5 minutes in lysis buffer (20 mM Tris pH 8.0 (RT), 100 mM NaCl, 20 mM
504 Imidazole pH 8.0 (RT), 5% Glycerol (v/v), 2 mM βMe, protease inhibitors (Millipore
505 Protease Inhibitor Cocktail Set III, Animal-Free)). The lysed solution underwent sonication
506 for 5 minutes prior to Triton-X being added to 0.1% (v/v). The solution was then
507 centrifuged at 20,000 g for 45 minutes at 2°C. The supernatant was then loaded onto a
508 HisTrap FF Crude column (Cytiva), washed with High Salt buffer (20 mM Tris pH 8.0 (RT),
509 1 M NaCl, 20 mM Imidazole pH 8.0 (RT), 5% Glycerol (v/v), 2 mM βMe), NiNTA A buffer
510 (20 mM Tris pH 8.0 (RT), 100 mM NaCl, 20 mM Imidazole pH 8.0 (RT), 5% Glycerol (v/v),
511 2 mM βMe), 6% NiNTA B, and eluted with NiNTA B (20 mM Tris pH 8.0 (RT), 100 mM
512 NaCl, 250 mM Imidazole pH 8.0 (RT), 5% Glycerol (v/v), 2 mM βMe). The eluent was
513 loaded onto a 5 mL StrepTrap column pre-equilibrated in GFB (20 mM HEPES pH 7.5
514 (RT), 150 mM NaCl, 5% Glycerol, 0.5 mM TCEP) and washed with GFB containing 0.5
515 M NaCl, an ATP wash (GFB with 2 mM ATP, 10 mM $MgCl_2$, and 150 mM KCl, a GFB
516 wash, and then eluted with GFB containing 2.5 mM desthiobiotin. Protein was
517 concentrated and injected onto a pre-equilibrated Superdex 200 10/300 column
518 equilibrated in GFB. Fractions containing protein were collected, aliquoted, flash frozen
519 in liquid nitrogen, and stored at -80°C.
520
521 ***PI4KA complex-Calcineurin size exclusion chromatography co-elution***
522 PI4KA complex (1.89 μM) and Calcineurin (8.17 μM) were incubated on ice for 15 minutes
523 prior to loading onto a Superose 6 Increase column pre-equilibrated in GFB [150 mM
524 NaCl, 20 mM imidazole (pH 7.0), 5% glycerol (v/v), 0.5 mM TCEP]. Fractions containing
525 the PI4KA complex bound to Calcineurin were pooled, concentrated, flash frozen in liquid
526 nitrogen and stored at -80°C. Fresh protein was run on an SDS-PAGE gel.
527
528 ***Electron Microscopy/Model Building***
529 *Protein sample preparation using BS^3 crosslinker:* PI4KA complex and Calcineurin were
530 incubated together on ice for 15 minutes at 2 μM and 4 μM, respectively. BS3 was added
531 to a final concentration of 1 mM and the reaction was incubated on ice for 2 hours. 1 M

532 Tris (pH 7.5) was added to 50 mM to quench the reaction and incubated at RT for 15
533 minutes. The quenched reaction was loaded onto Superose 6 Increase 10/300 column in
534 GFB [150 mM NaCl, 20 mM imidazole (pH 7.0), 5% glycerol (v/v), 0.5 mM TCEP].
535 Fractions encompassing the main peak, consistent with an elution volume of the complex,
536 were collected, concentrated, flash frozen in liquid nitrogen, and stored at -80°C.
537
538 *Cryo-EM sample preparation and data collection:* C-Flat 2/1-3Cu-T-50 grids were glow-
539 discharged for 25 s at 15 mA using a Pelco easiGlow glow discharger. 3 μl of PI4KA
540 complex crosslinked to Calcineurin were applied to the grids at 0.77 mg/ml and vitrified
541 using a Vitrobot Mark IV (FEI) by blotting for 1 second at a blot force of -5 at 4°C and
542 100% humidity. Specimens were screened using a 200-kV Glacios transmission
543 microscope (Thermo Fisher Scientific) equipped with a Falcon 3EC direct electron
544 detector (DED). Datasets were collected using a 300-kV Titan Krios equipped with a
545 Falcon 4i camera and the Selectris energy filter. A total of 10,121 super-resolution movies
546 were collected using SerialEM with a total dose of 50 e^{-}/Å^{2} over 603 frames at a physical
547 pixel size of 0.77 Å per pixel, using a defocus range of -1 to -2 um, at 165,000 x
548 magnification.
549
550 *Cryo-EM image processing:* All data processing was carried out using cryoSPARC v4.2.1.
551 Patch motion correction using default settings was applied to all movies to align the
552 frames and Fourier-crop the outputs by a factor of 2. The contrast transfer function (CTF)
553 of the resulting micrographs was estimated using the patch CTF estimation job with
554 default settings. Micrographs were manually curated to contain only micrographs with
555 CTF fit resolution less than or equal to 10.
556 To generate an initial model, 222,684 particles were picked from 2784 micrographs
557 using blob picking with a minimum and maximum diameter of 250 and 280, respectively.
558 Particles were inspected using the inspect picks job to remove particles that picked ice
559 contamination and were then extracted with a box size of 480 pixels and a Fourier
560 cropping of the output by a factor of 4, for a total of 154,266 particles. The particles were
561 subjected to two rounds of 2D classification. A total of 43,673 particles were used for *ab*

562 *initio* reconstruction and heterogeneous refinement using two classes, with C1 symmetry.
563 The best heterogeneous refinement then underwent one round of homogeneous
564 refinement with C1 symmetry. This was used to create 2D templates using cryoSPARC's
565 create templates job, which were used to pick particles from the complete dataset.
566 To generate a cryo-EM map from the complete dataset, the above 2D templates
567 were low pass filtered to 20 Å and used to template pick 9,830 micrographs with the
568 particle diameter set to 450 Å. 1,181,312 particles were inspected and 604,191 were
569 extracted with a box size of 1200 pixels and the outputs were Fourier-cropped by a factor
570 of 2.08, and subjected to 2D classification with 40 online-EM iterations to remove particles
571 with ice contamination or those who showed no features. 428,725 particles were used for
572 *ab initio* reconstruction and heterogeneous refinement using two classes and C1
573 symmetry. 239,931 particles from the best reconstruction underwent local motion
574 correction and a subsequent *ab initio* reconstruction and heterogeneous refinement with
575 two classes. A total of 235,760 particles were used to carry out a homogeneous
576 refinement with C1 symmetry using the previous 3D reconstruction as the starting model,
577 yielding a reconstruction with an overall resolution of 3.51 Å based on the Fourier shell
578 correlation (FSC) 0.143 criterion. Further refinement of these particles utilizing
579 homogenous refinement, Global CTF Correction and two rounds of non-uniform
580 refinement with C2 symmetry applied yielded a reconstruction with an overall resolution
581 of 3.50 Å based on the Fourier shell correlation (FSC) 0.143. The full workflow to generate
582 the final cryo-EM map is shown in Extended Figure 1.
583
584 *AlphaFold:* We used the protein prediction software, AlphaFold3 [30] to predict where
585 Calcineurin interacts with both PI4KA and FAM126A.
586 We first modelled the PI4KA interface using the AlphaFold server (BETA)
587 (https://golgi.sandbox.google.com/) and input the sequence of our
588 PI4KA/TTC7B/FAM126A ΔC complex construct and our Calcineurin construct (CNA
589 alpha 1 (2-391) and CNB) with cofactors (Fe^{2+}, 4 x Ca^{2+}). The resulting top ranked model
590 had ptm and iptm scores of 0.76 and 0.74, respectively, consistent with a stable complex.
591 To evaluate the confidence of individual subunit assembly predictions, based on our

592 previous knowledge from previously published X-ray and Cryo-EM structure of
593 TTC7B/FAM126A and PI4KA/TTC7B/FAM126A, respectively, we analyzed the
594 chain_pair_iptm and chain_pair_pae_min values. The chain_pair_iptm scores are useful
595 in evaluating the confidence of predicted protein-protein interfaces. The chain_pair_iptm
596 score for PI4KA:TTC7B was 0.84, TTC7B:FAM126A was 0.89, PI4KA:CNA was 0.72,
597 PI4KA:CNB was 0.54 and CNA:Fe^{2+} was 0.91. The chain_pair_pae_min values correlate
598 with whether two chain interact with each other. The chain_pair_pae_min score for
599 PI4KA:CNA was 3.39, and PI4KA:CNB was 11.24. The predicated aligned error (PAE)
600 for the top-ranked output is shown in Figure 3B. These metrics correlate with previously
601 published structural information and our Cryo-EM and HDX-MS data therefore we were
602 confident with this predicted model.
603 To predict the interaction between Calcineurin and FAM126A's C-terminus, we
604 used Alphafold3 with a search composed of the C-terminus of FAM126A (aa 390-521)
605 with Calcineurin (CNA alpha: aa 2-391, and CNB) with cofactors (4 x Ca^{2+}). The resulting
606 top ranked model had ptm and iptm scores of 0.81 and 0.76. The predicted aligned error
607 (PAE) for the top-ranked output is shown in Figure 5B. The chain_pair_iptm score for
608 FAM126ACterm:CNA was 0.74 and for FAM126ACterm:CNB was 0.63. The
609 chain_pair_pae_min score for FAM126ACterm:CNA was 2.39, and FAM126ACterm:CNB
610 was 3.85.
611
612 *Model building:* The cryo-EM structure of PI4KA-TTC7B-FAM126A (PDB: 6BQ1) [10] was
613 fit into the map using Chimera [42]. The horn domain of PI4KA was at higher local resolution
614 than the original data, and allowed for iterative rounds of automated model building in
615 Phenix guided by secondary structure predicted by AlphaFold [24], manual model building
616 in COOT, and refinement in Phenix.real_space_refine using realspace, rigid body, and
617 adp refinement with tight secondary structure restraints [43]. This allowed for building the
618 full solenoid horn domain with high confidence.
619 The local resolution of Calcineurin was the lowest of any protein chains, although
620 the high resolution structure of Calcineurin (PDB: 6NUC) [26] could be fit into the density.
621 We then used the AlphaFold3 search result for Calcineurin bound to the beta strand of

622 PI4KA (see previous section), and fit into the map using Chimera [42]. The entire model
623 was refined using Phenix.real_space_refine using rigid body, adp refinement with both
624 reference model restraints using the high resolution Calcineurin model 6NUC and tight
625 secondary structure restraints [43]. The full refinement and validation statistics are shown
626 in Supplementary Table 1.
627
628 ***HDX-MS***
629 *HDX-MS sample preparation:* Initial HDX reactions comparing PI4KA complex apo and
630 Calcineurin apo to PI4KA complex + Calcineurin were carried out in an 8.16 μl reaction
631 volume containing 11 pmol of both proteins. The exchange reactions were initiated by the
632 addition of 5.88 μL of D_2O buffer (20 mM Imidazole pH 7, 150 mM NaCl, 93.9% D_2O (V/V))
633 to 2.88 μL of protein (final D_2O concentration of 67.7%). Reactions proceeded for 3s, 30s,
634 and 300s at room temperature (18°C) before being quenched with ice cold acidic quench
635 buffer, resulting in a final concentration of 0.6M guanidine HCl and 0.9% formic acid post
636 quench. HDX reactions comparing PI4KA complex apo to PI4KA complex + Calcineurin
637 were then carried out at pH 6.5 to capture changes in disordered and flexible regions of
638 the PI4KA complex. Reactions occurred in an 8.12 μl reaction volume containing 10 pmol
639 of PI4KA complex and 20 pmol of Calcineurin. The exchange reactions were initiated by
640 the addition of 5.74 μL of D_2O buffer (20 mM MES pH 6.5, 150 mM NaCl, 1 mM $CaCl_2$,
641 93.37% D_2O (V/V)) to 2.38 μL of protein (final D_2O concentration of 67%). Reactions
642 proceeded for 3s, 10s, and 30s at 0°C before being quenched with ice cold acidic quench
643 buffer, resulting in a final concentration of 0.6M guanidine HCl and 0.9% formic acid post
644 quench. All conditions and time points were created and run in independent triplicate.
645 Samples were flash frozen immediately after quenching and stored at -80°C.
646 HDX reactions comparing FAM126A (415-521) apo to FAM126A (415-521) +
647 Calcineurin were carried out in a 12 μl reaction volume containing 30 pmol of both
648 proteins. The exchange reactions were initiated by the addition of 9 μL of D_2O buffer (20
649 mM MES pH 6.5, 150 mM NaCl, 1mM $CaCl_2$, 93.4% D_2O (V/V)) to 3 μL of protein (final
650 D_2O concentration of 70%). Reactions proceeded for 3s, 10s, and 30s at 0°C, pH 6.5
651 before being quenched with ice cold acidic quench buffer, resulting in a final concentration

652 of 0.6M guanidine HCl and 0.9% formic acid post quench. All conditions and time points
653 were created and run in independent triplicate. A fully deuterated sample was made
654 according to the protocol of [44] by incubating 1 μl of 30 μM FAM126A (415-521) with 7 M
655 guanidine HCl (final 4.67M), heated to 90°C for five minutes followed by two minutes
656 20°C, followed by the addition of 9 μl of D_2O buffer (20 mM MES pH 6.5, 150 mM NaCl,
657 1 mM $CaCl_2$, 93.37% D_2O (V/V)) for 10 minutes at 50°C then two minutes at 20°C, and
658 then 0°C for 2 minutes before being quenched as above. Samples were flash frozen
659 immediately after quenching and stored at -80°C.
660
661 *Protein digestion and MS/MS data collection:* Protein samples were rapidly thawed and
662 injected onto an integrated fluidics system containing a HDx-3 PAL liquid handling robot
663 and climate-controlled (2°C) chromatography system (Trajan), a Dionex Ultimate 3000
664 UHPLC system (Thermofisher), or a Acquity UPLC I-Class Series System (Waters), as
665 well as an Impact HD QTOF Mass spectrometer (Bruker). The full details of the automated
666 LC system are described in [28]. Samples comparing PI4KA complex apo and Calcineurin
667 apo to PI4KA complex + Calcineurin (pH 7.0, 18°C) were run over one immobilized pepsin
668 column (Trajan; ProDx protease column, 2.1 mm x 30 mm, PDX.PP01-F32) at 200 μL/min
669 for 3 minutes at 10°C. Samples comparing FAM126A (415-521) apo to FAM126A (415-
670 521) + Calcineurin and samples comparing PI4KA complex apo to PI4KA complex +
671 Calcineurin (pH 6.5, 0°C) were run over an immobilized pepsin column (Affipro; AP-PC-
672 001) at 200 μL/min for 4 minutes at 2°C. The resulting peptides were collected and
673 desalted on a C18 trap column (ACQUITY UPLC BEH C18 1.7 μm column, 2.1 mm x 5
674 mm; Waters 186004629). The trap was subsequently eluted in line with an ACQUITY 1.7
675 μm particle, 2.1 mm × 100 mm C18 UPLC column (Waters; 186003686), using a gradient
676 of 3-35% B (Buffer A 0.1% formic acid; Buffer B 100% acetonitrile) over 11 minutes
677 immediately followed by a gradient of 35-80% over 5 minutes. Mass spectrometry
678 experiments were acquired over a mass range from 150 to 2200 m/z using an
679 electrospray ionization source operated at a temperature of 200°C and a spray voltage of
680 4.5 kV.
681

682 *Peptide identification:* Peptides were identified from the non-deuterated samples of the
683 PI4KA complex, Calcineurin, or FAM126A (415-521) using data-dependent acquisition
684 following tandem MS/MS experiments (0.5 s precursor scan from 150-2000 m/z; twelve
685 0.25 s fragment scans from 150-2000 m/z). For HDX reactions comparing PI4KA complex
686 apo and Calcineurin apo to PI4KA complex + Calcineurin (pH 7.0, 18°C), MS/MS datasets
687 were analysed using PEAKS7 (PEAKS), and peptide identification was carried out by
688 using a false discovery based approach, with a threshold set to 0.1% using a database
689 of purified proteins and known contaminants [45]. The search parameters were set with a
690 precursor tolerance of 20 ppm, fragment mass error 0.02 Da, charge states from 1-8, with
691 a -10logP score of 31.9 and 15 for the PI4KA complex or Calcineurin respectively.
692 For HDX reactions comparing PI4KA complex apo to PI4KA complex + Calcineurin at pH
693 6.5, and FAM126A (415-521) apo to FAM126A (415-521) in complex with Calcineurin,
694 MS/MS datasets were analysed using FragPipe v18.0 and peptide identification was
695 carried out by using a false discovery-based approach using a database of purified
696 proteins and known contaminants [46–48]. MSFragger was utilised, and the precursor mass
697 tolerance error was set to -20 to 20 ppm. The fragment mass tolerance was set at 20
698 ppm. Protein digestion was set as nonspecific, searching between lengths of 4 and 50
699 aa, with a mass range of 400 to 5000 Da. For the Sf9 expressed PI4KA complex the
700 search was carried out with variable phosphorylation of S, T, and Y. Phosphorylated sites
701 in the PI4KA complex were identified in PI4KA between residues 252-281 and in TTC7B
702 residues 153-164, with these sites being 35% and 50% percent phosphorylated,
703 respectively.
704
705 **Quantification and statistical analysis**
706 ***Mass Analysis of Peptide Centroids and Measurement of Deuterium Incorporation***
707 HD-Examiner Software (Sierra Analytics) was used to automatically calculate the
708 level of deuterium incorporation into each peptide. All peptides were manually inspected
709 for correct charge state, correct retention time, appropriate selection of isotopic
710 distribution, etc. Deuteration levels were calculated using the centroid of the experimental
711 isotope clusters. Results are presented as relative levels of deuterium incorporation and

712 the only control for back exchange in the PI4KA complex containing experiments was the
713 level of deuterium present in the buffer (67.7% and 67%). For FAM126A (415-521) HDX
714 experiments, back exchange was controlled for by generating a fully deuterated sample.
715 For all HDX-MS experiments, differences in exchange in a peptide were considered
716 significant if they met all three of the following criteria: ≥5% change in exchange, ≥0.45
717 Da difference in exchange, and a p value <0.01 using a two tailed student t-test. The raw
718 HDX data are shown in two different formats. The raw peptide deuterium incorporation
719 graphs for a selection of peptides with significant differences are shown in Figures
720 3C/4D/S4B-E/S4G, with the raw data for all analysed peptides in the source data. To
721 allow for visualization of differences across all peptides, we utilised number of deuteron
722 difference (#D) plots (Fig. 4E/5E/S4A/S4F). These plots show the total difference in
723 deuterium incorporation over the entire H/D exchange time course, with each point
724 indicating a single peptide. Samples were only compared within a single experiment and
725 were never compared to experiments completed at a different time with a different final
726 D_2O level. The data analysis statistics for all HDX-MS experiments are in the source data
727 file according to the guidelines of [49]. The mass spectrometry proteomics data have been
728 deposited to the ProteomeXchange Consortium via the PRIDE partner repository [50] with
729 the dataset identifiers PXD043409 and PXD050633.
730
731 **Data and code availability**
732 • The EM data have been deposited in the EM data bank with accession number
733 (EMDB: 44382), and the associated structural model has been deposited to the
734 PDB with accession number (PDB: 9B9G). The MS proteomics data have been
735 deposited to the ProteomeXchange Consortium via the PRIDE [50] partner
736 repository with the dataset identifiers PXD043409 and PXD050633. All raw data in
737 all figures are available in the source data excel file.
738 • This paper does not report original code.
739 • Any additional information required to reanalyze the data reported in this paper is
740 available from the lead contact upon request.
741

742 **Acknowledgements**

743 JEB is supported by the Natural Science and Engineering Research council (Discovery
744 grant NSERC-2020-04241), and a Michael Smith Foundation for Health Research
745 (Scholar Award 17686). ALS was supported by an NSERC CGS-M scholarship. C.K.Y. is
746 supported by CIHR (PJT-168907) and the Natural Sciences and Engineering Research
747 Council of Canada (RGPIN-2018-03951). Cryo-EM specimens were prepared, and data
748 was collected at the High Resolution Macromolecular Electron Microscopy (HRMEM)
749 facility at the University of British Columbia (https://cryoem.med.ubc.ca). We thank Claire
750 Atkinson, Joeseph Felt, Liam Worrall and Natalie Strynadka. HRMEM is funded by the
751 Canadian Foundation for Innovation and the British Columbia Knowledge Development
752 Fund. We thank Dr. Martha Cyert for their insight and suggestions in the preparation of
753 the manuscript and for gifting us the GST Calcineurin expression vector.

754

755 **Author contributions**

756 Conceptualization, A.L.S., S.S., and J.E.B.; data curation, A,L.S., S.S., MLJ and
757 M.A.H.P.; formal analysis A.L.S., S.S., M.A.H.P., M.L.J., and J.E.B.; investigation A.L.S.,
758 S.S., M.A.H.P., N.J.H., M.L.J, and J.E.B.; visualization, A.L.S., S.S. and JEB; writing –
759 original draft, A.L.S., S.S., and J.E.B.; writing – reviewing and editing, A.L.S., S.S.,
760 M.A.H.P., N.J.H., M.L.J., C.K.Y., and J.E.B.; methodology, A.L.S., M.A.H.P, M.L.J.,
761 C.K.Y., and J.E.B.; supervision, C.K.Y., and J.E.B.; funding acquisition, C.K.Y., and
762 J.E.B.; project administration, J.E.B.

763

764 **Declaration of interest**

765 J.E.B. reports personal fees from Scorpion Therapeutics and Reactive therapeutics; and
766 research contracts from Novartis and Calico Life Sciences.

767

768 **References**

769 1. Hammond, G.R.V., and Burke, J.E. (2020). Novel roles of phosphoinositides in
770 signaling, lipid transport, and disease. Curr Opin Cell Biol *63*, 57–67.
771 https://doi.org/10.1016/j.ceb.2019.12.007.

2. Balla, T. (2013). Phosphoinositides: tiny lipids with giant impact on cell regulation. Physiol. Rev. *93*, 1019–1137. https://doi.org/10.1152/physrev.00028.2012.
3. Burke, J.E., Triscott, J., Emerling, B.M., and Hammond, G.R.V. (2023). Beyond PI3Ks: targeting phosphoinositide kinases in disease. Nat Rev Drug Discov *22*, 357–386. https://doi.org/10.1038/s41573-022-00582-5.
4. Batrouni, A.G., and Baskin, J.M. (2021). The chemistry and biology of phosphatidylinositol 4-phosphate at the plasma membrane. Bioorg Med Chem *40*, 116190. https://doi.org/10.1016/j.bmc.2021.116190.
5. Boura, E., and Nencka, R. (2015). Phosphatidylinositol 4-kinases: Function, structure, and inhibition. Exp. Cell Res. https://doi.org/10.1016/j.yexcr.2015.03.028.
6. Dornan, G.L., McPhail, J.A., and Burke, J.E. (2016). Type III phosphatidylinositol 4 kinases: structure, function, regulation, signalling and involvement in disease. Biochemical Society Transactions *44*, 260–266. https://doi.org/10.1042/BST20150219.
7. Pemberton, J.G., Kim, Y.J., Humpolickova, J., Eisenreichova, A., Sengupta, N., Toth, D.J., Boura, E., and Balla, T. (2020). Defining the subcellular distribution and metabolic channeling of phosphatidylinositol. J Cell Biol *219*, e201906130. https://doi.org/10.1083/jcb.201906130.
8. Zewe, J.P., Miller, A.M., Sangappa, S., Wills, R.C., Goulden, B.D., and Hammond, G.R.V. (2020). Probing the subcellular distribution of phosphatidylinositol reveals a surprising lack at the plasma membrane. J Cell Biol *219*, e201906127. https://doi.org/10.1083/jcb.201906127.
9. Chung, J., Torta, F., Masai, K., Lucast, L., Czapla, H., Tanner, L.B., Narayanaswamy, P., Wenk, M.R., Nakatsu, F., and De Camilli, P. (2015). INTRACELLULAR TRANSPORT. PI4P/phosphatidylserine countertransport at ORP5- and ORP8-mediated ER-plasma membrane contacts. Science *349*, 428–432. https://doi.org/10.1126/science.aab1370.
10. Lees, J.A., Zhang, Y., Oh, M.S., Schauder, C.M., Yu, X., Baskin, J.M., Dobbs, K., Notarangelo, L.D., De Camilli, P., Walz, T., et al. (2017). Architecture of the human

801 PI4KIIIα lipid kinase complex. Proc Natl Acad Sci U S A *114*, 13720–13725.
802 https://doi.org/10.1073/pnas.1718471115.
803 11. Dornan, G.L., Dalwadi, U., Hamelin, D.J., Hoffmann, R.M., Yip, C.K., and Burke, J.E.
804 (2018). Probing the Architecture, Dynamics, and Inhibition of the
805 PI4KIIIα/TTC7/FAM126 Complex. J. Mol. Biol. *430*, 3129–3142.
806 https://doi.org/10.1016/j.jmb.2018.07.020.
807 12. Baskin, J.M., Wu, X., Christiano, R., Oh, M.S., Schauder, C.M., Gazzerro, E.,
808 Messa, M., Baldassari, S., Assereto, S., Biancheri, R., et al. (2016). The
809 leukodystrophy protein FAM126A (hyccin) regulates PtdIns(4)P synthesis at the
810 plasma membrane. Nat. Cell Biol. *18*, 132–138. https://doi.org/10.1038/ncb3271.
811 13. Suresh, S., and Burke, J.E. (2023). Structural basis for the conserved roles of PI4KA
812 and its regulatory partners and their misregulation in disease. Adv Biol Regul *90*,
813 100996. https://doi.org/10.1016/j.jbior.2023.100996.
814 14. Baird, D., Stefan, C., Audhya, A., Weys, S., and Emr, S.D. (2008). Assembly of the
815 PtdIns 4-kinase Stt4 complex at the plasma membrane requires Ypp1 and Efr3. J
816 Cell Biol *183*, 1061–1074. https://doi.org/10.1083/jcb.200804003.
817 15. Nakatsu, F., Baskin, J.M., Chung, J., Tanner, L.B., Shui, G., Lee, S.Y., Pirruccello,
818 M., Hao, M., Ingolia, N.T., Wenk, M.R., et al. (2012). PtdIns4P synthesis by PI4KIIIα
819 at the plasma membrane and its impact on plasma membrane identity. J Cell Biol
820 *199*, 1003–1016. https://doi.org/10.1083/jcb.201206095.
821 16. Wu, X., Chi, R.J., Baskin, J.M., Lucast, L., Burd, C.G., De Camilli, P., and Reinisch,
822 K.M. (2014). Structural insights into assembly and regulation of the plasma
823 membrane phosphatidylinositol 4-kinase complex. Developmental Cell *28*, 19–29.
824 https://doi.org/10.1016/j.devcel.2013.11.012.
825 17. Barlow-Busch, I., Shaw, A.L., and Burke, J.E. (2023). PI4KA and PIKfyve: Essential
826 phosphoinositide signaling enzymes involved in myriad human diseases. Curr Opin
827 Cell Biol *83*, 102207. https://doi.org/10.1016/j.ceb.2023.102207.
828 18. Bigorgne, A.E., Farin, H.F., Lemoine, R., Mahlaoui, N., Lambert, N., Gil, M., Schulz,
829 A., Philippet, P., Schlesser, P., Abrahamsen, T.G., et al. (2014). TTC7A mutations

830 disrupt intestinal epithelial apicobasal polarity. J Clin Invest *124*, 328–337.
831 https://doi.org/10.1172/JCI71471.
832 19. Zara, F., Biancheri, R., Bruno, C., Bordo, L., Assereto, S., Gazzerro, E., Sotgia, F.,
833 Wang, X.B., Gianotti, S., Stringara, S., et al. (2006). Deficiency of hyccin, a newly
834 identified membrane protein, causes hypomyelination and congenital cataract. Nat.
835 Genet. *38*, 1111–1113. https://doi.org/10.1038/ng1870.
836 20. Salter, C.G., Cai, Y., Lo, B., Helman, G., Taylor, H., McCartney, A., Leslie, J.S.,
837 Accogli, A., Zara, F., Traverso, M., et al. (2021). Biallelic PI4KA variants cause
838 neurological, intestinal and immunological disease. Brain *144*, 3597–3610.
839 https://doi.org/10.1093/brain/awab313.
840 21. Verdura, E., Rodríguez-Palmero, A., Vélez-Santamaria, V., Planas-Serra, L., de la
841 Calle, I., Raspall-Chaure, M., Roubertie, A., Benkirane, M., Saettini, F., Pavinato, L.,
842 et al. (2021). Biallelic PI4KA variants cause a novel neurodevelopmental syndrome
843 with hypomyelinating leukodystrophy. Brain *144*, 2659–2669.
844 https://doi.org/10.1093/brain/awab124.
845 22. Ulengin-Talkish, I., and Cyert, M.S. (2023). A cellular atlas of calcineurin signaling.
846 Biochim Biophys Acta Mol Cell Res *1870*, 119366.
847 https://doi.org/10.1016/j.bbamcr.2022.119366.
848 23. Ulengin-Talkish, I., Parson, M.A.H., Jenkins, M.L., Roy, J., Shih, A.Z.L., St-Denis,
849 N., Gulyas, G., Balla, T., Gingras, A.-C., Várnai, P., et al. (2021). Palmitoylation
850 targets the calcineurin phosphatase to the phosphatidylinositol 4-kinase complex at
851 the plasma membrane. Nat Commun *12*, 6064. https://doi.org/10.1038/s41467-021-
852 26326-4.
853 24. Jumper, J., Evans, R., Pritzel, A., Green, T., Figurnov, M., Ronneberger, O.,
854 Tunyasuvunakool, K., Bates, R., Žídek, A., Potapenko, A., et al. (2021). Highly
855 accurate protein structure prediction with AlphaFold. Nature *596*, 583–589.
856 https://doi.org/10.1038/s41586-021-03819-2.
857 25. Baek, M., DiMaio, F., Anishchenko, I., Dauparas, J., Ovchinnikov, S., Lee, G.R.,
858 Wang, J., Cong, Q., Kinch, L.N., Schaeffer, R.D., et al. (2021). Accurate prediction

859 of protein structures and interactions using a three-track neural network. Science
860 *373*, 871–876. https://doi.org/10.1126/science.abj8754.
861 26. Hendus-Altenburger, R., Wang, X., Sjøgaard-Frich, L.M., Pedraz-Cuesta, E.,
862 Sheftic, S.R., Bendsøe, A.H., Page, R., Kragelund, B.B., Pedersen, S.F., and Peti,
863 W. (2019). Molecular basis for the binding and selective dephosphorylation of
864 Na+/H+ exchanger 1 by calcineurin. Nat Commun *10*, 3489.
865 https://doi.org/10.1038/s41467-019-11391-7.
866 27. Masson, G.R., Jenkins, M.L., and Burke, J.E. (2017). An overview of hydrogen
867 deuterium exchange mass spectrometry (HDX-MS) in drug discovery. Expert Opin
868 Drug Discov *12*, 981–994. https://doi.org/10.1080/17460441.2017.1363734.
869 28. Stariha, J.T.B., Hoffmann, R.M., Hamelin, D.J., and Burke, J.E. (2021). Probing
870 Protein–Membrane Interactions and Dynamics Using Hydrogen–Deuterium
871 Exchange Mass Spectrometry (HDX-MS). In Protein-Ligand Interactions: Methods
872 and Applications Methods in Molecular Biology., T. Daviter, C. M. Johnson, S. H.
873 McLaughlin, and M. A. Williams, eds. (Springer US), pp. 465–485.
874 https://doi.org/10.1007/978-1-0716-1197-5_22.
875 29. Parson, M.A.H., Jenkins, M.L., and Burke, J.E. (2022). Investigating how intrinsically
876 disordered regions contribute to protein function using HDX-MS. Biochem Soc Trans
877 *50*, 1607–1617. https://doi.org/10.1042/BST20220206.
878 30. Abramson, J., Adler, J., Dunger, J., Evans, R., Green, T., Pritzel, A., Ronneberger,
879 O., Willmore, L., Ballard, A.J., Bambrick, J., et al. (2024). Accurate structure
880 prediction of biomolecular interactions with AlphaFold 3. Nature *630*, 493–500.
881 https://doi.org/10.1038/s41586-024-07487-w.
882 31. Brauer, B.L., Moon, T.M., Sheftic, S.R., Nasa, I., Page, R., Peti, W., and Kettenbach,
883 A.N. (2019). Leveraging New Definitions of the LxVP SLiM To Discover Novel
884 Calcineurin Regulators and Substrates. ACS Chem Biol *14*, 2672–2682.
885 https://doi.org/10.1021/acschembio.9b00606.
886 32. Wigington, C.P., Roy, J., Damle, N.P., Yadav, V.K., Blikstad, C., Resch, E., Wong,
887 C.J., Mackay, D.R., Wang, J.T., Krystkowiak, I., et al. (2020). Systematic Discovery

888 of Short Linear Motifs Decodes Calcineurin Phosphatase Signaling. Mol Cell *79*,
889 342-358.e12. https://doi.org/10.1016/j.molcel.2020.06.029.
890 33. Coales, S.J., E, S.Y., Lee, J.E., Ma, A., Morrow, J.A., and Hamuro, Y. (2010).
891 Expansion of time window for mass spectrometric measurement of amide
892 hydrogen/deuterium exchange reactions. Rapid Commun. Mass Spectrom. *24*,
893 3585–3592. https://doi.org/10.1002/rcm.4814.
894 34. Li, Y., Sheftic, S.R., Grigoriu, S., Schwieters, C.D., Page, R., and Peti, W. (2020).
895 The structure of the RCAN1:CN complex explains the inhibition of and substrate
896 recruitment by calcineurin. Sci. Adv. *6*, eaba3681.
897 https://doi.org/10.1126/sciadv.aba3681.
898 35. Czirják, G., and Enyedi, P. (2014). The LQLP calcineurin docking site is a major
899 determinant of the calcium-dependent activation of human TRESK background K+
900 channel. J Biol Chem *289*, 29506–29518. https://doi.org/10.1074/jbc.M114.577684.
901 36. Li, H., Pink, M.D., Murphy, J.G., Stein, A., Dell'Acqua, M.L., and Hogan, P.G. (2012).
902 Balanced interactions of calcineurin with AKAP79 regulate Ca2+-calcineurin-NFAT
903 signaling. Nat Struct Mol Biol *19*, 337–345. https://doi.org/10.1038/nsmb.2238.
904 37. Hornbeck, P.V., Zhang, B., Murray, B., Kornhauser, J.M., Latham, V., and Skrzypek,
905 E. (2015). PhosphoSitePlus, 2014: mutations, PTMs and recalibrations. Nucleic
906 Acids Res. *43*, D512-20. https://doi.org/10.1093/nar/gku1267.
907 38. McPhail, J.A., Ottosen, E.H., Jenkins, M.L., and Burke, J.E. (2017). The Molecular
908 Basis of Aichi Virus 3A Protein Activation of Phosphatidylinositol 4 Kinase IIIβ,
909 PI4KB, through ACBD3. Structure *25*, 121–131.
910 https://doi.org/10.1016/j.str.2016.11.016.
911 39. Burke, J.E. (2018). Structural Basis for Regulation of Phosphoinositide Kinases and
912 Their Involvement in Human Disease. Mol. Cell *71*, 653–673.
913 https://doi.org/10.1016/j.molcel.2018.08.005.
914 40. Dornan, G.L., Stariha, J.T.B., Rathinaswamy, M.K., Powell, C.J., Boulanger, M.J.,
915 and Burke, J.E. (2020). Defining How Oncogenic and Developmental Mutations of
916 PIK3R1 Alter the Regulation of Class IA Phosphoinositide 3-Kinases. Structure *28*,
917 145-156.e5. https://doi.org/10.1016/j.str.2019.11.013.

41. Gouet, P., Robert, X., and Courcelle, E. (2003). ESPript/ENDscript: Extracting and rendering sequence and 3D information from atomic structures of proteins. Nucleic Acids Res. *31*, 3320–3323.
42. Pettersen, E.F., Goddard, T.D., Huang, C.C., Couch, G.S., Greenblatt, D.M., Meng, E.C., and Ferrin, T.E. (2004). UCSF Chimera--a visualization system for exploratory research and analysis. J Comput Chem *25*, 1605–1612. https://doi.org/10.1002/jcc.20084.
43. Afonine, P.V., Grosse-Kunstleve, R.W., Echols, N., Headd, J.J., Moriarty, N.W., Mustyakimov, M., Terwilliger, T.C., Urzhumtsev, A., Zwart, P.H., and Adams, P.D. (2012). Towards automated crystallographic structure refinement with phenix.refine. Acta Crystallogr. D Biol. Crystallogr. *68*, 352–367. https://doi.org/10.1107/S0907444912001308.
44. Peterle, D., Wales, T.E., and Engen, J.R. (2022). Simple and Fast Maximally Deuterated Control (maxD) Preparation for Hydrogen-Deuterium Exchange Mass Spectrometry Experiments. Anal Chem *94*, 10142–10150. https://doi.org/10.1021/acs.analchem.2c01446.
45. Dobbs, J.M., Jenkins, M.L., and Burke, J.E. (2020). Escherichia coli and Sf9 Contaminant Databases to Increase Efficiency of Tandem Mass Spectrometry Peptide Identification in Structural Mass Spectrometry Experiments. J Am Soc Mass Spectrom *31*, 2202–2209. https://doi.org/10.1021/jasms.0c00283.
46. Kong, A.T., Leprevost, F.V., Avtonomov, D.M., Mellacheruvu, D., and Nesvizhskii, A.I. (2017). MSFragger: ultrafast and comprehensive peptide identification in mass spectrometry-based proteomics. Nat Methods *14*, 513–520. https://doi.org/10.1038/nmeth.4256.
47. da Veiga Leprevost, F., Haynes, S.E., Avtonomov, D.M., Chang, H.-Y., Shanmugam, A.K., Mellacheruvu, D., Kong, A.T., and Nesvizhskii, A.I. (2020). Philosopher: a versatile toolkit for shotgun proteomics data analysis. Nat Methods *17*, 869–870. https://doi.org/10.1038/s41592-020-0912-y.
48. Dobbs, J.M., Jenkins, M.L., and Burke, J.E. (2020). Escherichia coli and Sf9 Contaminant Databases to Increase Efficiency of Tandem Mass Spectrometry

Peptide Identification in Structural Mass Spectrometry Experiments. J Am Soc Mass Spectrom *31*, 2202–2209. https://doi.org/10.1021/jasms.0c00283.

49. Masson, G.R., Burke, J.E., Ahn, N.G., Anand, G.S., Borchers, C., Brier, S., Bou-Assaf, G.M., Engen, J.R., Englander, S.W., Faber, J., et al. (2019). Recommendations for performing, interpreting and reporting hydrogen deuterium exchange mass spectrometry (HDX-MS) experiments. Nat. Methods *16*, 595–602. https://doi.org/10.1038/s41592-019-0459-y.
50. Perez-Riverol, Y., Bai, J., Bandla, C., García-Seisdedos, D., Hewapathirana, S., Kamatchinathan, S., Kundu, D.J., Prakash, A., Frericks-Zipper, A., Eisenacher, M., et al. (2022). The PRIDE database resources in 2022: a hub for mass spectrometry-based proteomics evidences. Nucleic Acids Res *50*, D543–D552. https://doi.org/10.1093/nar/gkab1038.

986 **Supplemental Figures Tables**

987 **Table S1 Cryo-EM data collection, refinement, and validation statistics**

	EMDB: 44382 PDB: 9B9G
Data collection and processing	
Magnification	165,000
Voltage (kV)	300
Electron exposure (e/ Å^2)	50
Defocus range (μM)	1.0-2.0
Pixel size (Å)	0.77
Symmetry imposed	C2
Initial particle images (no.)	604,191
Final particle images (no.)	235,760
Map resolution (Å)	3.5
FSC threshold	0.143
Map resolution range (Å)	3.3-10
Refinement	
Initial model used (PDB)	6BQ1,6NUC
Model Resolution (Å)	3.5
FSC threshold	0.143
Map sharpening B factor	
Model composition	
Non-hydrogen atoms	48,676
Protein residues	6075
Ligands	8
B-factors	
Protein	195.7
Validation	
Mol probability score	2.18
Clashscore	11.90
Poor rotamers (%)	2.24
Ramachandran	
Favored	95.32
Allowed	4.68
Outliers	0.00
R.m.s. deviations	
Bond lengths (Å)	0.003
Bond angles (°)	0.730

988
989
990
991

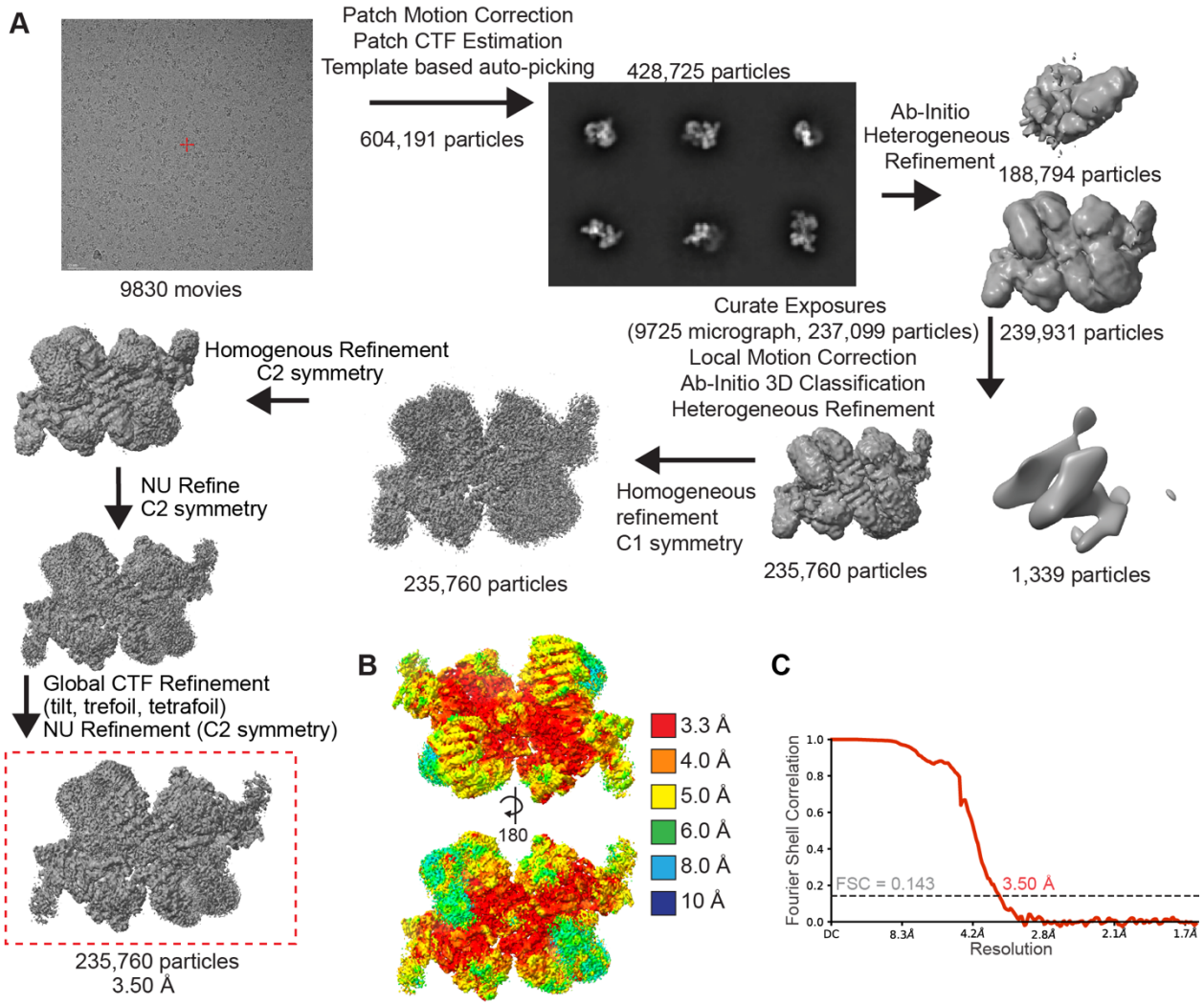

Supplemental Figure 1. Cryo-EM data processing

A. Cryo-EM data processing workflow showing a representative micrograph from screening on the 200 kV Glacios, representative 2D class averages, and the image processing strategy used to generate a 3D reconstruction of the PI4KA/TTC7B/FAM126A/Calcineurin complex.

B. Final PI4KA/TTC7B/FAM126A/ Calcineurin map coloured according to local resolution estimated using cryoSPARC v4.2.1 (FSC threshold 0.143)

C. Gold standard Fourier shell correlation coefficient (FSC) curve after auto tightening by cryoSPARC for the PI4KA/TTC7B/FAM126A/ Calcineurin map.

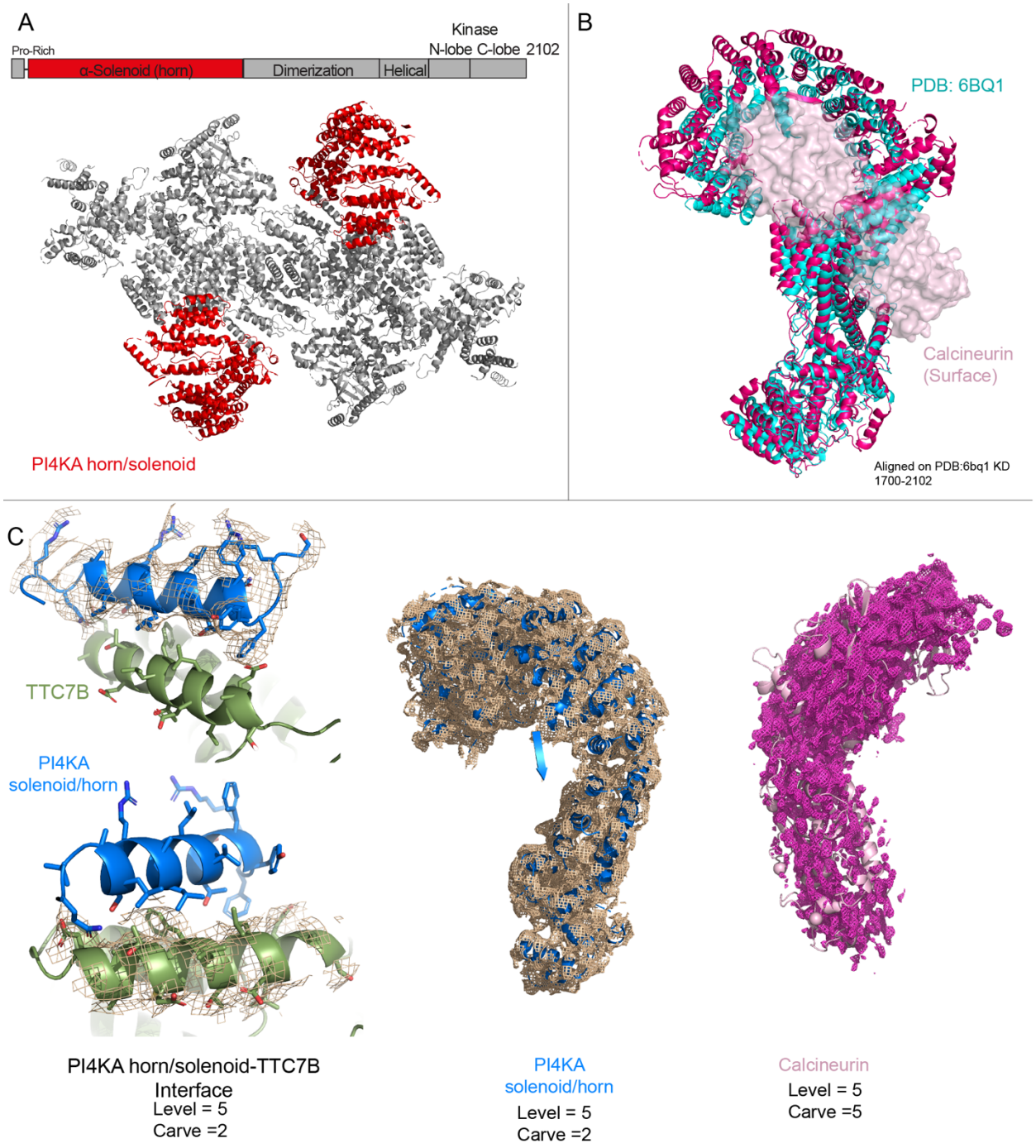

Supplemental Figure 2. Model density fit

A. Unique features in the PI4KA complex resolved from the cryo-EM map of the PI4KA complex interacting with Calcineurin. Red areas represent unique features, annotated on the domain schematic, and mapped onto the structural model with Calcineurin removed.

B. Comparison of the PI4KA structure from our study (magenta) to PI4KA from PI4KA/TTC7B/FAM126A (2-289) (cyan) apo (PDB:6BQ1) (Lees *et al*, 2017). Our model was aligned to 6BQ1 using residues 1700-2102.

C. Electron density of selected regions. (L) TTC7B-PI4KA solenoid/horn interface, with density for the N-terminal helix of PI4KA shown on top, and the density for the TTC7B interface helix shown on bottom (M) PI4KA solenoid/horn (aa 27-929), and (R) Calcineurin.

A

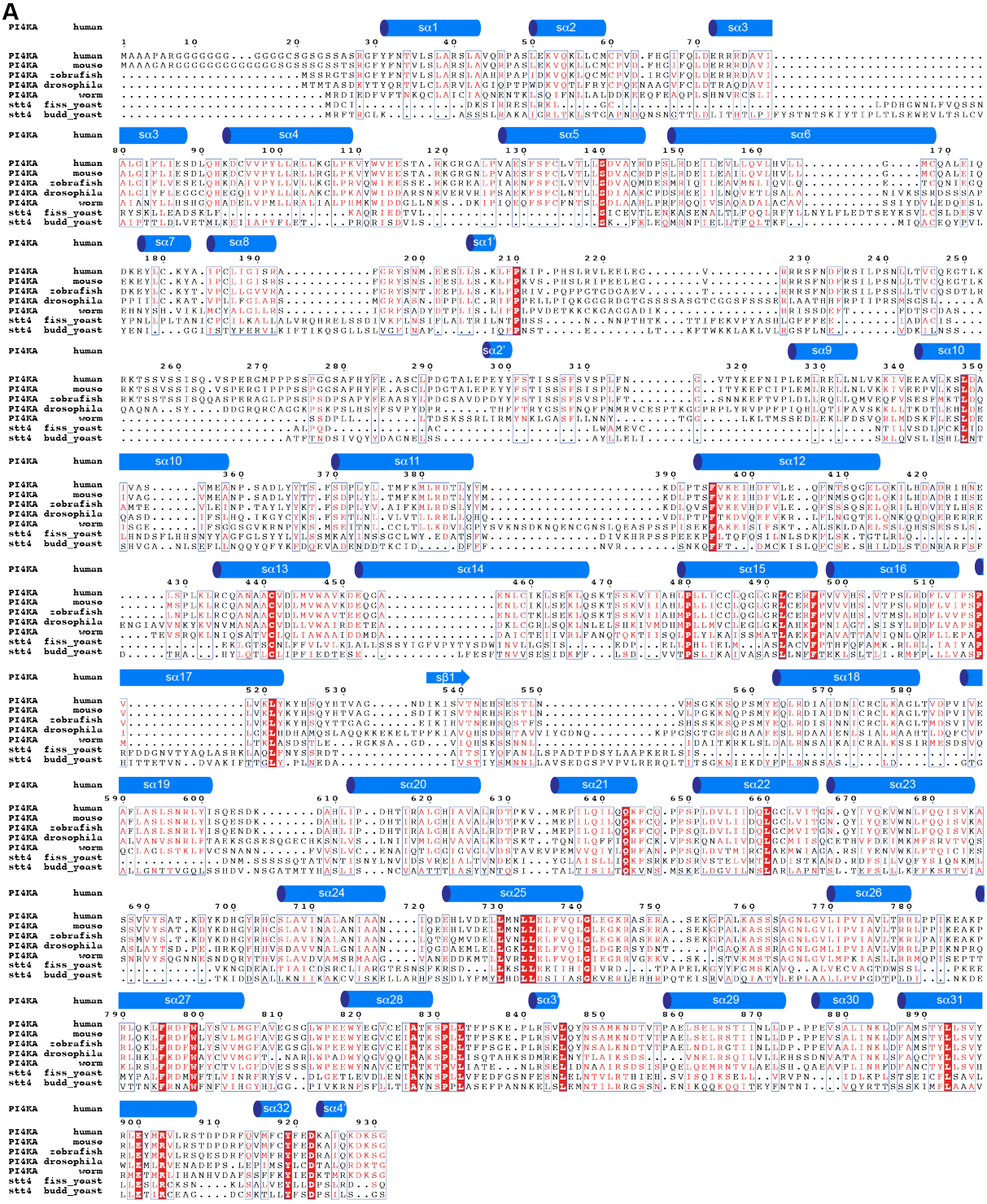

Supplemental Figure 3. Secondary structure annotation of PI4KA solenoid/horn

A. Multiple sequence alignment (generated with ESPript 3.0) of PI4KA from *Homo sapiens, Mus musculus, Danio rerio, Drosophila melanogaster, Caenorhabditis elegans*, *Schizosaccharomyces pombe,* and *Saccharomyces cerevisiae.* Secondary structure elements from the human PI4KA horn region, as determined from the cryo-EM map of the PI4KA complex bound to Calcineurin, are illustrated above the alignment.

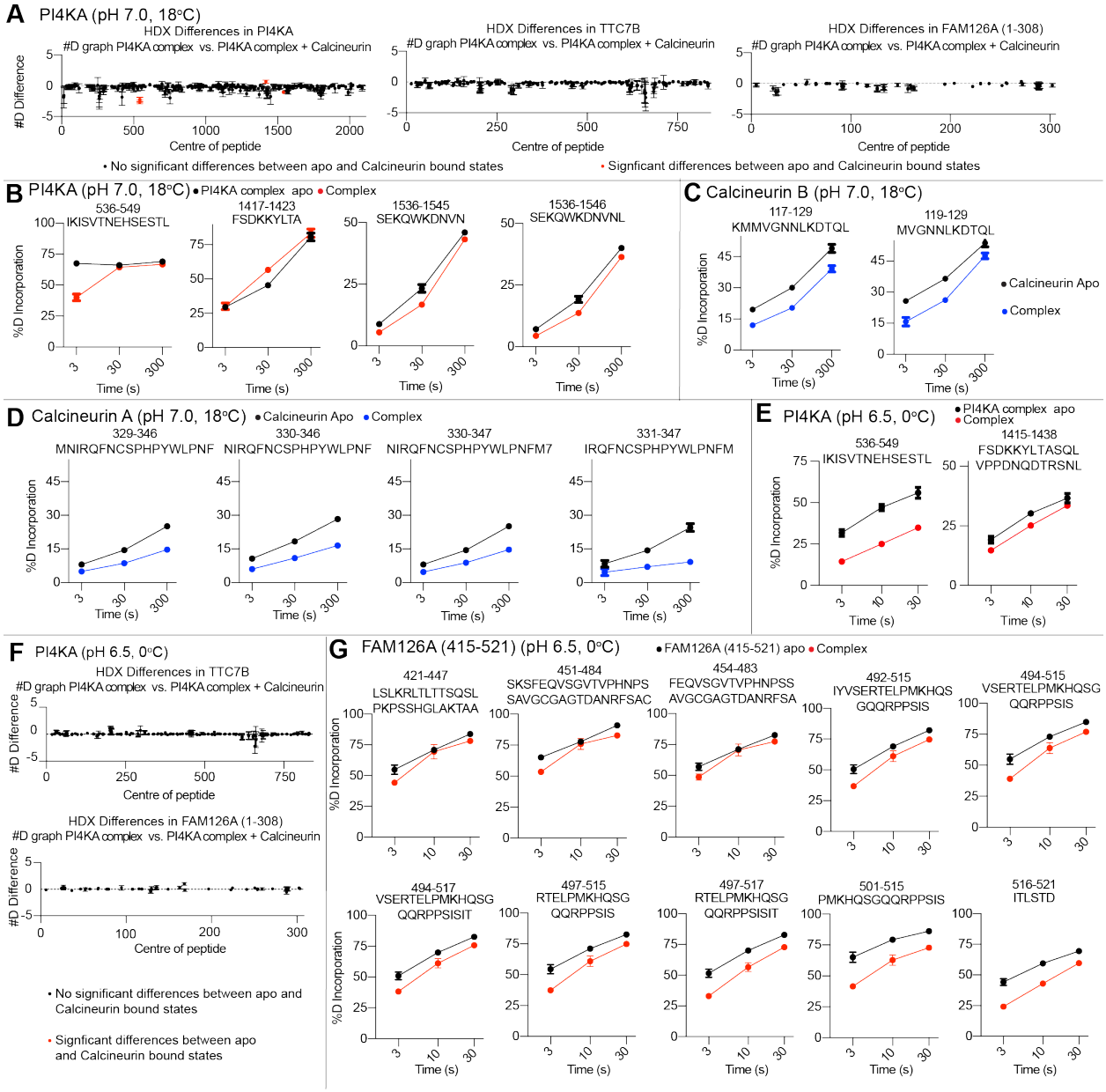

Supplemental Figure 4. HDX-MS data underlying all experiments

A. Sum of the number of deuteron difference of (L) PI4KA, (M) TTC7B, and (R) FAM126A (1-308) upon complex formation with Calcineurin analysed over the entire deuterium exchange time course (pH 7.0, 18°C). Each point is representative of the centre residue of an individual peptide. Peptides that met the significance criteria (see panels **B**) are colored red. Error is shown as standard deviation (SD) (n=3). The full source data underlying all HDX-MS data is included as an excel file.

B. Selected deuterium exchange time courses of PI4KA peptides (pH 7.0, 18°C) that showed significant (defined as >5% 0.45 Da, and p<0.01 in an unpaired two-tailed t test at any time point) changes in exchange. Error is shown as standard deviation (SD) (n=3).

C. Selected deuterium exchange time courses of Calcineurin B peptides (pH 7.0, 18°C) that showed significant (defined as >5% 0.45 Da, and p<0.01 in an unpaired two-tailed t test at any time point) decreases in exchange. Error is shown as standard deviation (SD) (n=3).

D. Selected deuterium exchange time courses of Calcineurin A peptides (pH 7.0, 18°C) that showed significant (defined as >5% 0.45 Da, and p<0.01 in an unpaired two-tailed t test at any time point) decreases in exchange. Error is shown as standard deviation (SD) (n=3).

1036 **E.** Selected deuterium exchange time courses of PI4KA peptides (pH 6.5, 0°C) that showed significant
1037 (defined as >5% 0.45 Da, and $p<0.01$ in an unpaired two-tailed t test at any time point) decreases or
1038 increases in exchange. Error is shown as standard deviation (SD) (n=3).
1039 **F.** Sum of the number of deuteron difference of (L)TTC7B, and (R) FAM126A (1-308) upon complex
1040 formation with Calcineurin analysed over the entire deuterium exchange time course (pH 6.5, 0°C). Each
1041 point is representative of the centre residue of an individual peptide. Peptides that met the significance
1042 criteria (see panels **E**) are colored red. Error is shown as standard deviation (SD) (n=3). The full source
1043 data underlying all HDX-MS data is included as an excel file.
1044 **G.** Selected deuterium exchange time courses FAM 126A (415-521) peptides (pH 6.5, 0°C) that showed
1045 significant (defined as >5% 0.45 Da, and $p<0.01$ in an unpaired two-tailed t test at any time point) decreases
1046 or increases in exchange. Error is shown as standard deviation (SD) (n=3).
1047
1048
1049
1050
1051
1052

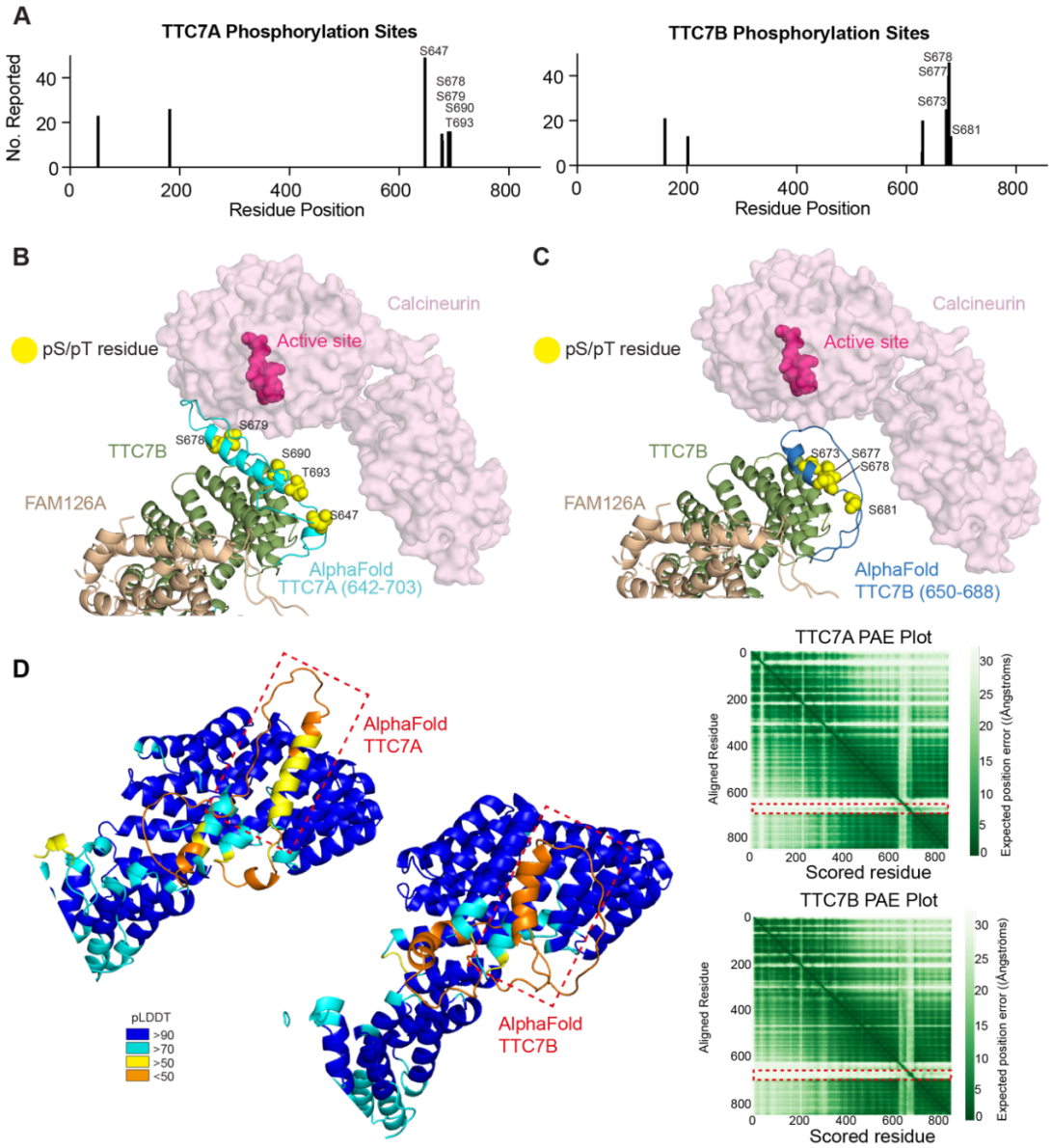

Supplemental Figure 5. AlphaFold modelling of TTC7A/B on cryo-EM structure reveals evolutionary conserved phosphorylation sites in TTC7A and TTC7B in close proximity to Calcineurin active site.
A. Phosphorylated serine/threonine residues in TTC7A (left) and TTC7B (right) reported on PhosphoSite (Hornbeck *et al*, 2015). Serine/threonine residues reported more than five times are shown.
B. Multiple reported TTC7A phosphorylation sites are in proximity to the Calcineurin active site. AlphaFold model of the disordered loop in TTC7A (642-703) is aligned to the experimental density for TTC7B. Threonine/serine residues reported to be phosphorylated are shown as yellow spheres. The AlphaFold model used for the alignment are shown in panel D.
C. Multiple reported TTC7B phosphorylation sites are in proximity to the Calcineurin active site. AlphaFold model of the disordered loop in TTC7B (650-688) is aligned to the experimental density for TTC7B. Threonine/serine residues reported to be phosphorylated are shown as yellow spheres. The AlphaFold model used for the alignment are shown in panel D.
D. (L) AlphaFold models of TTC7A and TTC7B coloured based on pLDDT according to the legend. The disordered loop not present in the experimental structure is boxed in red. The predicted alignment error (PAE) for both AlphaFold models are shown, with the areas boxed in red indicating the disordered loop in close proximity to Calcineurin in the PI4KA-TTC7-FAM126-Calcineurin structure.